ISSN 0458-2128

Communications
from the
University of London
Observatory
No. 79

A STUDY OF INTERSTELLAR UV LINES TOWARDS SIX MEMBERS OF THE SCO OB1 ASSOCIATION

by

Ian A. Crawford

February 1989

Department of Physics & Astronomy
University College London

Editorial

Communications from the University of London Observatory are original monographs published as an occasional series. They are sent free to the libraries of all institutions on the Observatory's list of exchange partners, or to institutions and individuals who request them by writing to the Editor at the address below.

Publication of *Communications from the University of London Observatory* is assisted by a gift to University College London in memory of Frank Norman Jenkins.

M. M. Dworetsky,
Editor

The Library
University of London Observatory
Mill Hill Park
London NW7 2QS
United Kingdom

CONTENTS

1 Summary

This paper describes a study of ultraviolet interstellar lines, observed with the *IUE* satellite, towards six stars in the Scorpius OB1 association. The equivalent widths of 75 lines, arising from 27 ionic species, are given for each star. Column densities, obtained by means of a curve of growth analysis, and the corresponding elemental depletions are also given. Density-dependent depletion may have been observed for the atoms Ca, Cr, Mn and Ni. Interstellar electron densities have been estimated from the observed column densities of successive ionisation stages of Mg, C and S, although these were found to be uncertain by several orders of magnitude ($-2 \lesssim \log n_e \lesssim +1$) because of saturation of the stronger lines. Limits were obtained to the gas pressure from an analysis of the excitation of the fine structure levels of neutral carbon; for all but one star $\log(P/k) \gtrsim 4$ cm^{-3} K, corresponding to a density $n_H \gtrsim 140$ cm^{-3} for an assumed temperature of 80 K.

2 The *IUE* data for Sco OB1

The *IUE* data base at the World Data Centre (Rutherford and Appleton Laboratory) was searched for high resolution *IUE* images of stars in the Sco OB1 association. Images were found to be available for the stars: HD 151804, 152234, 152235, 152236, 152408, and 152424. All available images (or up to a maximum of six in each wavelength range for stars with many images available) were de-archived and transferred to the UCL *Starlink* node. Table 1 lists the images used for each star.

Spectra were extracted from the images using the IUEDR program of Giddings (1983a,b). Once extracted, a number of corrections have to be made to the spectra and these are discussed below.

(1) *Zero level correction.* Because of the possible overlap of the échelle orders, care has to be taken to estimate the correct zero intensity level. An error in the zero level due to order-overlap manifests itself by the flat cores of saturated interstellar absorption lines lying *below* the nominal zero level. IUEDR incorporates a method for correcting order-overlap based on the observed intensity of the flat core of the interstellar Lyα line, and this was applied for all the SWP spectra in which Lyα could be discerned. For the HD 152235 and HD 152236 SWP images there was no measurable flux at Lyα and the default correction (Giddings 1983a) was applied. There is no corresponding procedure for estimating the zero level for the LWR images, although the effect of order-overlap in this wavelength range is thought to be less serious (Giddings 1983a). In any case, any remaining zero-level error (in both wavelength regions) was estimated from the cores of the other saturated interstellar lines, and was generally found to be about 5%, except for the LWR spectra of HD 151804 & HD 152235 where a base level error of 10 % was adopted. These base level errors were incorporated into the errors quoted on the measured equivalent widths (see Section 4).

Table 1.

IUE images used for the analysis of the interstellar UV lines towards Sco OB1. The exposure times are also given.

Star (HD)	SWP	exp (s)	LWR	exp (s)
151804	2759	420	1556	240
	2760	420	2461	230
	2986	600	4466	220
	6301	462		
	9269	449		
152234	2147	1200	12471	270
	6488	1020		
	16206	540		
152235	16205	5400	12470	3000
152236	1892	3600	1892	720
	2103	2100	2290	660
	2507	5460	5250	340
	2987	2100		
	5659	1320		
152408	1624	720	1555	840
	2105	900	4465	540
	6141	900	11736	300
	6889	1200		
	6890	900		
	14936	840		
152424	2758	4200	2459	1200
	9719	4200	2460	1620
	15021	3600	11574	900

(2) *Wavelength calibration.* The measured wavelengths of spectral features will differ from their rest values because of the satellite's motion, the motion of the object, and an instrumental shift. Although a wavelength scale is provided, the accuracy of this calibration can only be determined by measuring the position of a feature with a known wavelength. In particular, the magnitude of the instrumental shift has to be determined and it is usual (Giddings 1983a) to make use of sharp interstellar lines with known laboratory wavelengths. Although this procedure is clearly unsatisfactory for the study of the interstellar lines themselves, it is the only reliable way of obtaining an accurate, self-consistent wavelength scale, and it does make it possible to measure any *relative* shifts that may exist between interstellar lines. Residual displacements of about ± 0.03Å were found to remain between the corrected and laboratory wavelengths of different lines after the wavelength calibration had been completed.

(3)*Ripple correction.* It is desirable to remove the effect of the échelle blaze function of each order from the final spectrum. Failure to do so properly will result in adjacent orders not 'joining up' with each other, leading to discontinuous jumps in the spectrum at the order boundaries. Default ripple corrections are applied by IUEDR, but these can only be considered as first approximations (Giddings 1983a) and are not always satisfactory. Barker (1984) has developed a method for ripple correction which has been incorporated into IUEDR by Dr. I. D. Howarth for SWP spectra, and has been used for all the SWP spectra in this study. This procedure is not available for the LWR images. However, since the interstellar line analysis is based on equivalent width measurements the effect of échelle ripple on the analysis is relatively unimportant since only the *local* continuum is required. In those cases where the effect of ripple was thought to be significant, the uncertainty was included in the estimated equivalent width errors.

Once calibrated, each spectrum was mapped onto a uniform wavelength grid at 0.05Å (SWP) and 0.10Å (LWR) intervals. Multiple spectra of the same wavelength range for a given star were then merged, weighted by an 'effective' exposure time given by $t_{eff} = t \times < F >$, where t is the actual exposure time (Table 1) and $< F >$ is the mean flux recorded in the spectrum (Dr. I. D. Howarth, personal communication).

The resolving power of the high resolution mode was given by Boggess *et al.* (1978a) as $R = 1.2 \times 10^4$ for the short wavelength range, and 1.3×10^4 for the long wavelength range. These correspond to velocity resolutions (FWHM of the instrumental response function) of 25 and 23 km s^{-1} respectively. There is, however, some uncertainty in the actual velocity resolution, and Howarth & Phillips (1986) adopted a value of 30 km s^{-1} (for both spectrographs) based on a comparison between observed line profiles and an empirical curve of growth analysis.

3 Velocity structure in the *IUE* spectra

High resolution observations (3 km s^{-1}, FWHM) of interstellar Na I and Ca II towards stars in the Sco OB1 association (Crawford, Barlow & Blades 1989) have revealed very complex velocity structure in the line profiles, and it is clearly of interest to see if any of it can be discerned in the lower resolution *IUE* spectra. It was found that, while the blue wings of some lines were shallower than the red (apparently indicating unresolved, blue-shifted absorption), most of the interstellar lines were roughly symmetrical. The majority of lines, though symmetrical, were found to be significantly broader than the nominal *IUE* response function of $\sim$30 km s^{-1} FWHM, which also suggests unresolved structure. In no cases were discrete velocity components resolved.

The effect of the broad *IUE* response function is illustrated graphically in Figure 1. Figure 1(a) shows the effect of convolving the optical spectrum of Na I (from Crawford *et al.* 1989) towards HD 152235 (solid line) with a Guassian of FWHM 30 km s^{-1}. All the detailed velocity structure is lost, leaving a single, broad, asymmetric profile (dashed line). For comparison the observed profile of the 2343.5 Å line of Fe II towards the same star is also shown (dotted line). Figure 1(b) shows the result of convolving the high resolution Na I spectrum of HD 152236 with a 30 km s^{-1} Gaussian. In this case the dotted curve is the observed profile of the 2852.1 Å line of Mg I.

From the above discussion it is clear that the *IUE* data are not capable of determining either the number of velocity components present towards these stars or their parameters (velocities, column densities and velocity dispersions). Given that the *IUE* instrumental response function is itself uncertain, by perhaps as much as $\pm$5 km s^{-1} (Section 2), it follows that a line profile analysis, of the kind performed by Crawford *et al.* (1989) for the high resolution observations of Na I and Ca II, would be of very limited value. Instead, we have obtained the atomic and ionic column densities have been obtained from equivalent width measurements and a curve of growth analysis. Such a procedure can, of course, only obtain the *total* column densities along each line of sight. The detailed study of atomic abundances in velocity components separated by only a few tens of km s^{-1} must await the availability of higher resolution UV spectrographs.

4 Equivalent width measurements

The equivalent widths of all the UV interstellar atomic lines given in the line list of Morton (1975), and that were visible in the spectra, were measured using the DIPSO program, described by Howarth & Murray (1988). Additional lines listed by Howarth & Phillips (1986), but not listed by Morton, were also included.

Table 2 gives the identifications, oscillator strengths and equivalent widths for the interstellar UV lines observed towards these six stars. Owing to the difficulty of fitting a polynomial to the local continuum for many regions of the

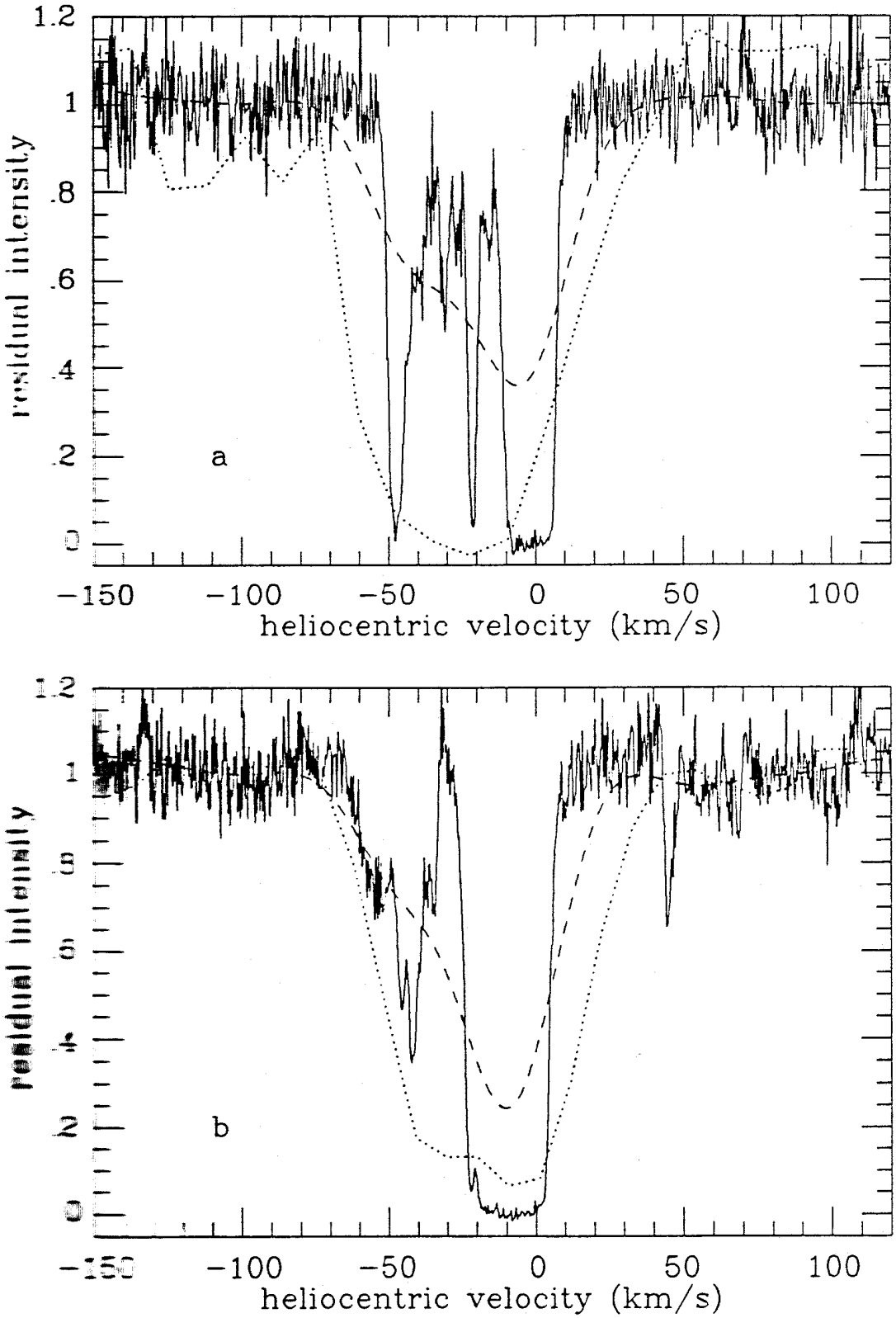

Figure 1. A demonstration of the limited velocity resolution available with *IUE*. (a) Solid line: optical spectrum ($R = 10^5$, Crawford *et al.* 1989) of the interstellar Na D2 line towards HD 152235; dashed line: optical spectrum convolved with a 36 km s^{-1} FWHM Gaussian to simulate the *IUE* resolution; dotted line: *IUE* observation of the 2343.5 Å line of Fe II towards this star. (b) As for (a) except towards HD 152236; dotted line: the 2852.1 Å line of Mg I towards this star.

spectra (because of poor signal/noise, line blanketing and, in particular, the occurrence of strong stellar-wind P-Cygni profiles), the errors quoted on the equivalent widths have been estimated from extreme high and low positions of the continuum. These errors are thought to be conservative. The continuum errors were combined with those resulting from the estimated zero level errors (Section 2) to obtain the quoted errors on the equivalent widths. Where it was possible to estimate reliable upper limits for non-observed lines these are given, but no attempt was made to estimate upper limits for lines that were not measurable because of lack of adequate exposure (*e.g.* at the extreme short wavelength end of some of the SWP images) or because they were masked by broad stellar or stellar-wind absorptions.

Many of the CI, C I*, and C I** (where an * indicates an excited hyperfine level in the ground state) are partially blended. It was, nevertheless, found to be possible to estimate the equivalent widths for these lines (with rather large errors that include the effect of the blend) and these lines are marked with an asterisk in the last column of Table 2. Several other lines (due to elements other than C I) were found to be so badly blended that it was not possible to estimate equivalent widths for the two components separately. For such cases the *total* equivalent width is given alongside one of the components (thought to be the dominant one) and a note in the last column identifies the other component.

Recently, Van Steenberg & Shull (1988) have published equivalent widths for the interstellar lines of Si II, Fe II, S II, Mn II and Zn II for four of the stars studied here: HD 151804, 152234, 152236 & 152408. In order to see if the present work is consistent with that of Van Steenberg & Shull, their equivalent widths are plotted against those obtained here for HD 151804 in Figure 2. It can be seen that the agreement is generally good, but that Van Steenberg & Shull's equivalent widths tend, on average, to be slightly larger than those obtained here. Since Van Steenberg & Shull's measurements were made from single exposures, whereas those given here are from multiple (merged) exposures, this effect may be due to the higher signal/noise ratio of the present work. Moreover, the errors quoted by Van Steenberg & Shull are 1σ values only, whereas those given here are extreme values (see above), so the vertical error bars in Figure 2 should probably be lengthened if they are to be compared with the horizontal ones. The equivalent widths for the other three stars common to both studies all show a similar agreement.

Since Van Steenberg & Shull (1988) used entirely different software from that employed here for their spectrum extraction and calibration, the agreement shown in Figure 2 gives one confidence that the procedures adopted in the present study are reliable.

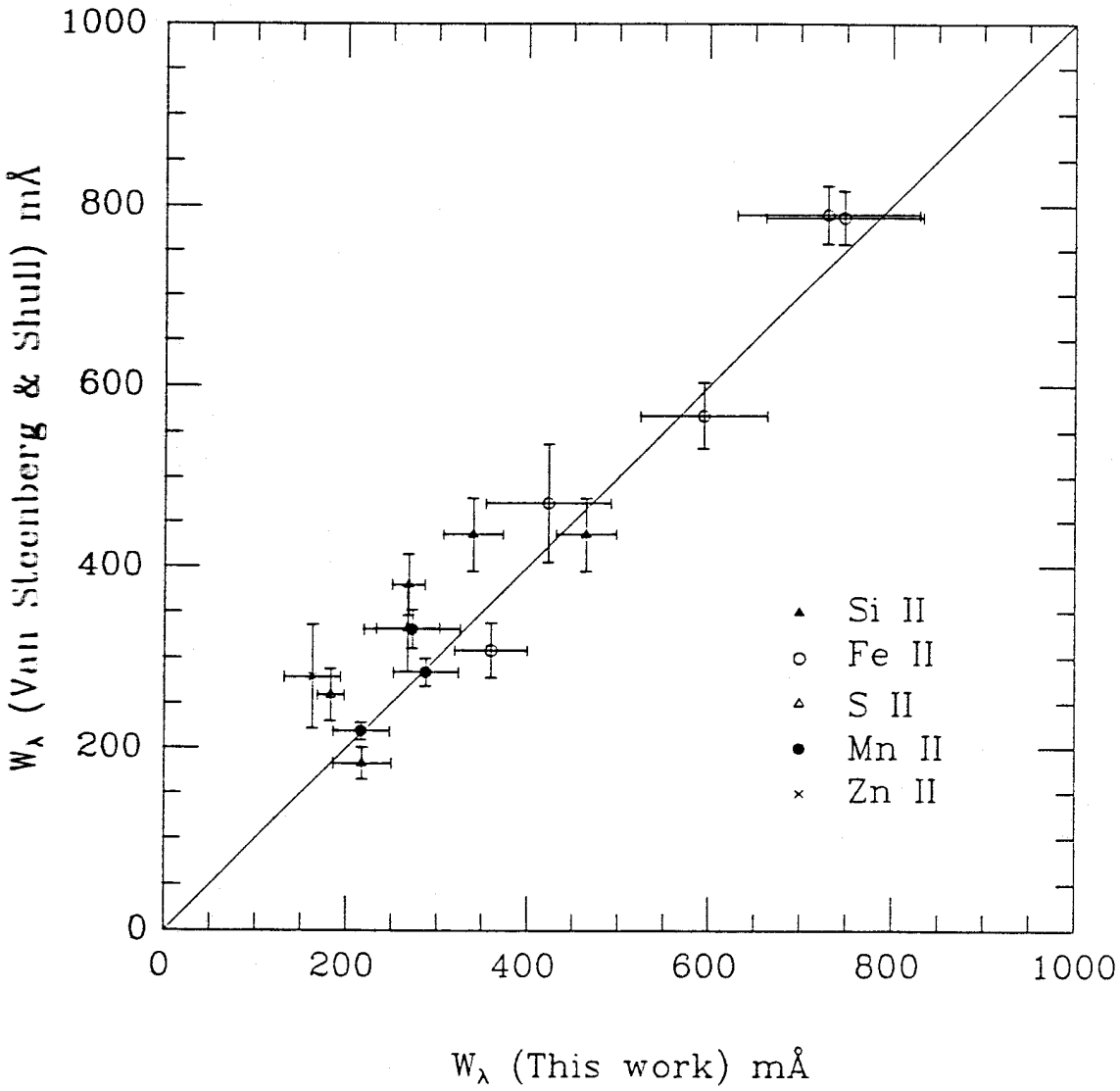

Figure 2. A comparison between the equivalent widths measured here and those given by Van Steenberg & Shull (1988) for HD 151804.

Table 2.

Equivalent widths for the interstellar atomic lines identified in the *IUE* spectra of six Sco OB1 stars. (Units are mÅ.)

Ion	λ(Å)	f	Ref	151804	152234	152235	152236	152408	152424	Comments
C I	1155.809	0.01700	1	100±15	...	...	...	168±51	...	
C I	1157.910	0.02200	1	87±28	...	...	...	131±35	...	
C I	1158.324	0.00340	1	...	...	...	...	75±20	...	
C I	1260.736	0.03790	1	...	...	...	...	...	...	bl. 1260.4 Si II
C I	1276.482	0.01200	1	≲10	32± 9	...	...	57±28	36± 5	*
C I	1277.245	0.15600	1	120±40	145±30	50±15	118±19	155±40	113±36	*
C I	1280.135	0.02780	1	74±26	95±25	≲100	103±46	99±30	93±33	*
C I	1328.833	0.08240	1	86±34	95±25	...	143±35	101±30	84±32	*
C I	1560.310	0.08100	1	124±34	194±75	129±58	155±39	205±35	176±55	*
C I*	1277.513	0.03900	1	28±18	84±26	43±12	59±20	47±28	68±35	*
C I*	1279.890	0.01200	2	...	43±16	...	70±40	...	52±22	*
C I*	1280.597	0.00920	2	...	...	...	...	...	32±14	*
C I*	1329.101	0.08240	1	26±14	89±26	...	121±32	64±17	79±36	*
C I*	1560.690	0.08100	2	68±32	159±56	150±53	165±48	110±27	179±44	*
C I**	1261.533	0.02840	3	...	44±20	≲16	...	...	37±13	
C I**	1279.498	0.00100	2	...	...	...	...	27±12	...	*
C I**	1329.584	0.08240	1	≲31	60±12	47±12	71±27	27±12	48±13	*
C I**	1561.438	0.06800	3	≲10	131±47	78±27	116±18	45±11	102±32	*

C I**	1561.438	0.06800	3	$\lesssim$10	131±47	78±27	116±18	45±11	102±32	*
C II	1334.532	0.11800	1	554±35	520±40	...	...	467±33	503±44	
C II*	1335.703	0.11800	1	420±30	402±45	400±50	335±40	413±33	413±38	
C IV	1548.188	0.19400	1	145±28	120±70	...	146±25	37±25	93±29	
N I	1199.550	0.13300	1	290±38	263±55	...	...	282±31	...	bl. 1199.4 Mn II
N I	1200.223	0.08850	1	...	216±20	...	...	245±41	...	
N I	1200.710	0.04420	1	...	189±15	...	...	272±38	...	
N V	1238.821	0.15200	1	...	$\lesssim$33	...	...	...	$\lesssim$8	
N V	1242.804	0.07570	1	$\lesssim$6	$\lesssim$23	...	$\lesssim$8	$\lesssim$9	...	
O I	1302.168	0.04860	1	433±32	440±38	500±100	...	442±40	434±42	
O I	1355.598	1.25E-6	1	$\lesssim$12	25± 8	...	...	$\lesssim$22	$\lesssim$9	
O I*	1304.858	0.04850	1	$\lesssim$4	$\lesssim$12	27±10	...	$\lesssim$8	13± 6	
O I**	1306.029	0.04850	1	13± 4	$\lesssim$12	$\lesssim$21	$\lesssim$29	...	15± 4	
Mg I	2025.824	0.11000	1	...	...	...	...	...	...	bl. 2025.5 Zn II
Mg I	2852.127	1.77000	1	550±75	684±65	...	628±44	703±57	627±50	
Mg II	1239.925	9.68E-4	1	51±17	92±18	...	83±23	26± 9	71±16	
Mg II	1240.395	4.84E-4	1	22± 9	71±19	...	43±11	19± 7	55±12	
Mg II	2795.528	0.59200	1	1145±125	1062±97	...	930±90	890±60	1136±98	
Mg II	2802.704	0.29500	1	1129±118	975±97	1034±150	884±80	861±64	1011±89	
Al II	1670.787	1.88000	1	540±44	480±50	456±43	440±54	505±74	515±60	

Table 2 (continued)

Ion	λ(Å)	f	Ref	151804	152234	152235	152236	152408	152424	Comments
Al III	1854.716	0.53900	1	220±30	212±26	194±20	130±35	155±23	...	
Al III	1862.790	0.26800	1	190±27	162±21	124±37	40±20	110±14	...	
Si II	1190.416	0.25100	1	519±32	...	...	...	450±73	472±81	
Si II	1193.289	0.50000	1	440±39	453±57	...	...	487±41	321±58	
Si II	1260.421	0.95900	1	578±52	480±54	...	450±50	570±100	520±80	bl. 1260.7 C I
Si II	1304.372	0.14700	1	340±33	322±33	285±60	340±36	321±26	296±28	
Si II	1526.708	0.07640	1	465±33	486±31	340±57	520±75	437±30	430±70	
Si II	1808.012	0.00371	1	218±32	273±30	310±50	304±35	310±27	292±60	* 1807.3 S I
Si III	1206.510	1.66000	1	393±40	313±58	...	...	380±35	280±100	
Si IV	1393.755	0.52800	1	48±10	30±11	62±16	...	23±11	39± 9	
Si IV	1402.770	0.26200	1	$\lesssim$20	$\lesssim$14	...	30±20	17± 4	28±16	
S I	1295.653	0.10800	1	$\lesssim$4	17± 3	$\lesssim$21	...	...	15±3	
S I	1316.533	0.04100	2	...	22± 7	$\lesssim$28	12± 5	$\lesssim$10	16± 5	
S I	1401.541	0.01580	2	$\lesssim$4	$\lesssim$18	...	...	$\lesssim$12	$\lesssim$13	
S I	1807.311	0.11200	2	29± 9	48±10	128±64	...	22± 9	55±33	* 1808.0 Si II
S II	1250.586	0.00535	1	183±15	221±25	190±40	300±23	249±26	211±37	
S II	1253.812	0.01070	1	268±35	282±33	320±95	260±35	247±23	218±27	
S II	1259.520	0.01590	1	269±18	267±24	225±37	...	297±23	240±38	
Cl I	1188.772	0.08810	1	97±34	88±18	...	...	80±22	...	

Cl I	1188.772	0.08810	1	97±34	88±18	...	...	80±22	...	
Cl I	1347.240	0.11200	1	41±10	88±11	40±12	90±20	69±16	83±11	
Cr II	2055.590	0.20300	1	84±8	...	...	130±27	102±10	67±7	
Mn II	1197.184	0.09600	1	51±8	63±23	180±80	130±23	...	50±17	
Mn II	1199.391	0.10000	1	...	...	...	...	...	...	bl. 1199.6 N I
Mn II	1201.118	0.05800	1	...	$\lesssim$50	...	$\lesssim$100	$\lesssim$100	$\lesssim$130	
Mn II	2576.105	0.28800	1	288±36	340±40	380±68	348±43	334±32	370±40	
Mn II	2593.731	0.22300	1	273±53	390±43	367±62	303±32	350±68	330±40	
Mn II	2606.697	0.15800	1	217±31	280±38	280±48	236±40	285±33	297±31	
Fe II	1608.456	0.09630	4	360±40	264±29	300±30	268±25	346±35	222±38	
Fe II	2343.495	0.15000	4	...	578±60	497±75	627±52	585±70	736±74	
Fe II	2373.733	0.04190	4	423±69	548±100	560±115	424±80	472±54	433±51	
Fe II	2382.034	0.39800	4	730±100	642±63	649±96	677±63	574±52	724±73	
Fe II	2585.876	0.08460	4	594±70	600±60	596±90	583±52	537±41	568±52	
Fe II	2599.395	0.29400	4	748±86	756±64	724±94	736±68	626±50	717±53	
Ni II	1370.136	0.10000	1	58± 7	51±11	56±18	74± 9	71±14	55±11	
Ni II	1393.330	0.01800	1	...	$\lesssim$12	$\lesssim$24	...	$\lesssim$5	$\lesssim$10	
Cu II	1358.773	0.46000	1	...	12± 4	$\lesssim$25	$\lesssim$20	...	32±16	
Zn II	2025.512	0.41200	1	287±15	537±49	647±49	728±130	451±37	530±49	bl. 2025.8 Mg I
Zn II	2062.016	0.20200	1	163±31	320±75	$\lesssim$800	124±26	265±28	340±91	

References for the oscillator strengths are: (1) Morton (1978); (2) Morton (1975); (3) Morton & Smith (1973); (4) Nussbaumer *et al.* (1981). A * in the last column indicates that the line is a partial blend but that the estimated errors include the likely effect of this; bl. indicates a close blend for which the individual equivalent widths cannot be estimated (see text).

5 Curve of growth analysis

5.1 The dominant H I region ions

Assuming that the degree of ionisation in the interstellar medium is maintained by UV photons in the interstellar radiation field, it follows that ions which require more than 13.6 eV to be created from a lower ionisation stage should not be found in H I clouds, because any significant amount of hydrogen will "mop up" photons with higher energies. On the other hand, H I clouds would be expected to be permeated with photons with energies <13.6 eV, and so atoms or ions with ionisation potentials less than this will occur predominantly in the next highest ionisation stage. It follows that the dominant ions expected in H I clouds are C II, N I, O I, Mg II, Al II, Si II, S II, Mn II, Fe II, Ni II, Cu II and Zn II (*cf.* Morton 1975).

Since these are expected to be the dominant ions, their lines can be used to define empirical curves of growth for the H I clouds. In practice it is necessary to have several lines well spaced in values of $\log(f\lambda)$ to define a curve of growth, and here we have followed Morton (1975) and used the observed lines of N I, Mg II, Si II, S II & Fe II. The other ions in the list above can then, fairly safely, be assumed to lie on the same curve of growth because they probably exist in the same regions along the line of sight.

The empirical curves of growth were obtained by plotting $\log(w_\lambda/\lambda)$, where w_λ is the equivalent width, against $\log(f\lambda)$ for the observed lines, and then shifting the groups of points for each ion horizontally (*i.e.* along the $\log(f\lambda)$ axis) until a smooth curve was defined. This was then compared with theoretical curves of growth calculated with the BACH program (due originally to Davenhall 1977, and incorporated into DIPSO by Dr. I. D. Howarth) in order to determine the velocity dispersion parameter b. The resulting curves are plotted in Figure 3. The solid line shown in each case is the theoretical curve of growth for the 2802.7 Å line of Mg II, and the horizontal axis has been labelled for this line. The b values used are indicated in the figures. The maximum uncertainty in the b value, due to the scatter of the points about the theoretical curve, was found to be about ± 2 km s^{-1} in each case.

The b values found in this way are all large, between 15 and 25 km s^{-1}, which clearly reflects unresolved velocity structure, rather than the b values of individual clouds. There is an anti-correlation between b value and reddening (Figure 4). Since one would expect there to be more clouds along a more highly reddened line of sight, which should lead to a larger effective b value owing to bulk velocity differences between them, this is contrary to initial expectations. It can be explained, however, by the increasing dominance of clouds with very low individual b values with increasing reddening. This reduces the overall *average* value given by the empirical curve of growth obtained from the equivalent widths of lines in which the sub-structure is not resolved.

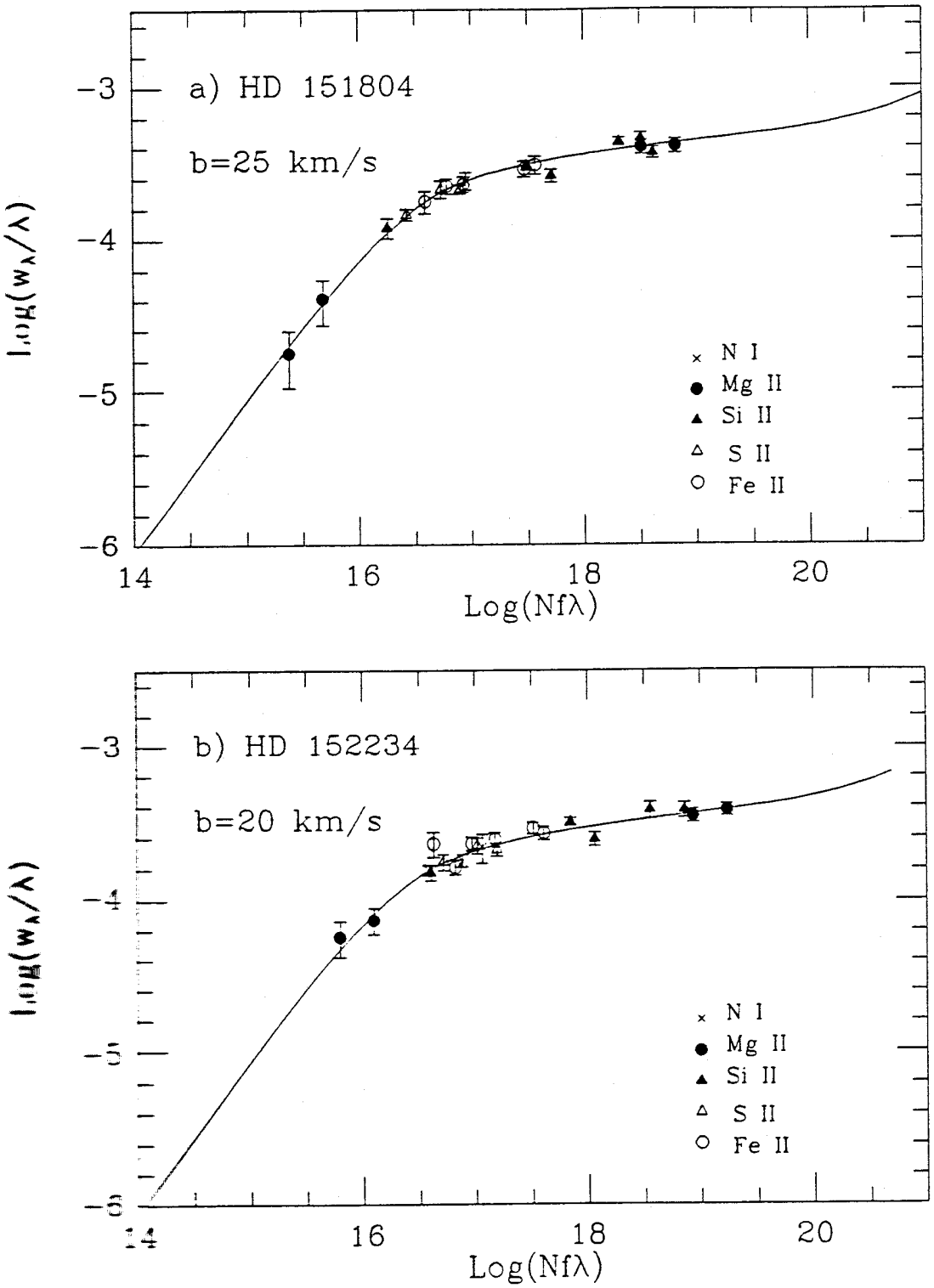

Figure 3(a,b). Empirical curves of growth for the interstellar lines towards HD 151804 and HD 152234. Solid lines are theoretical curves of growth with the b values indicated. See text for explanation.

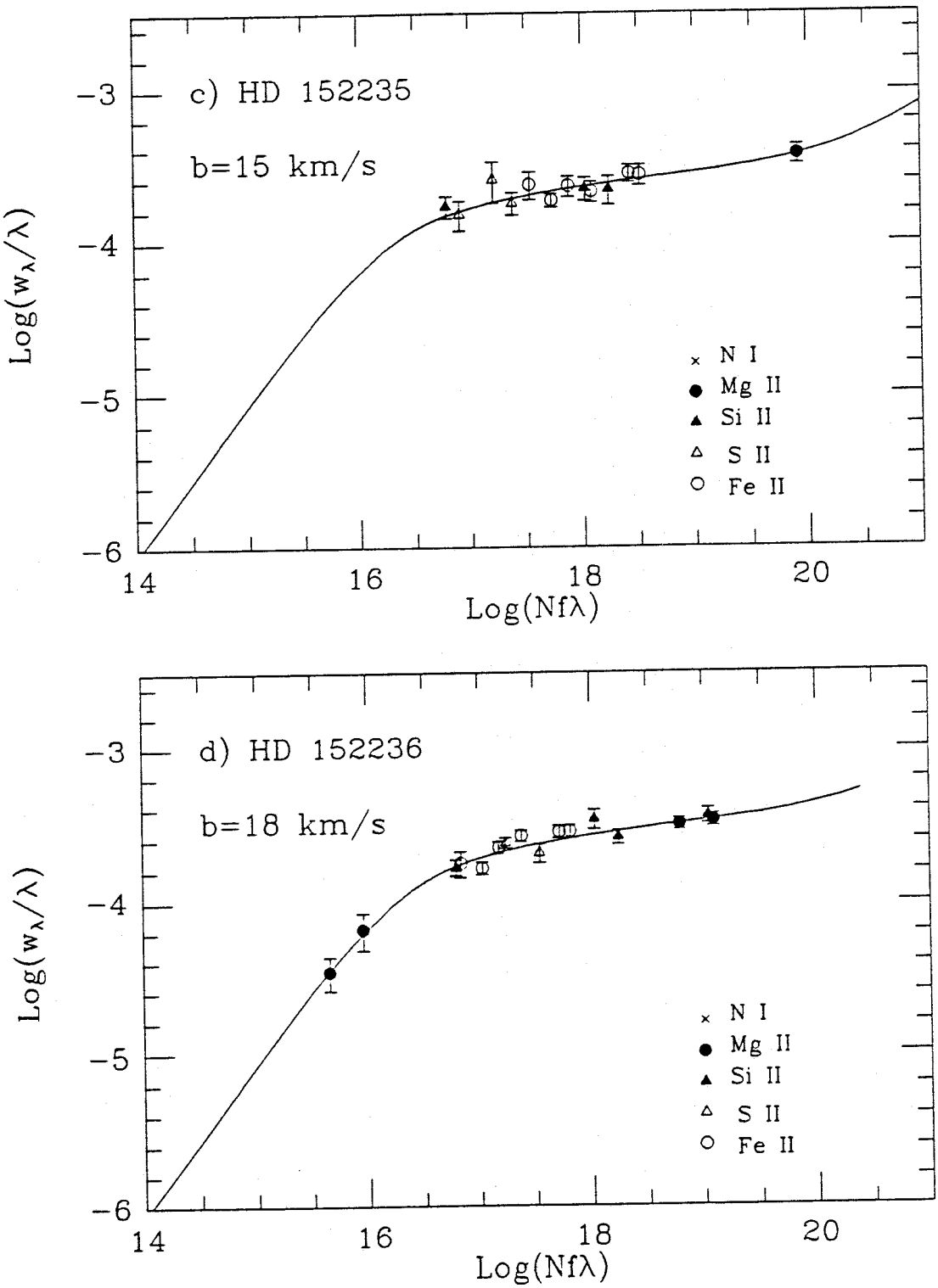

Figure 3(c,d). Empirical curves of growth for the interstellar lines towards HD 152235 and HD 152236.

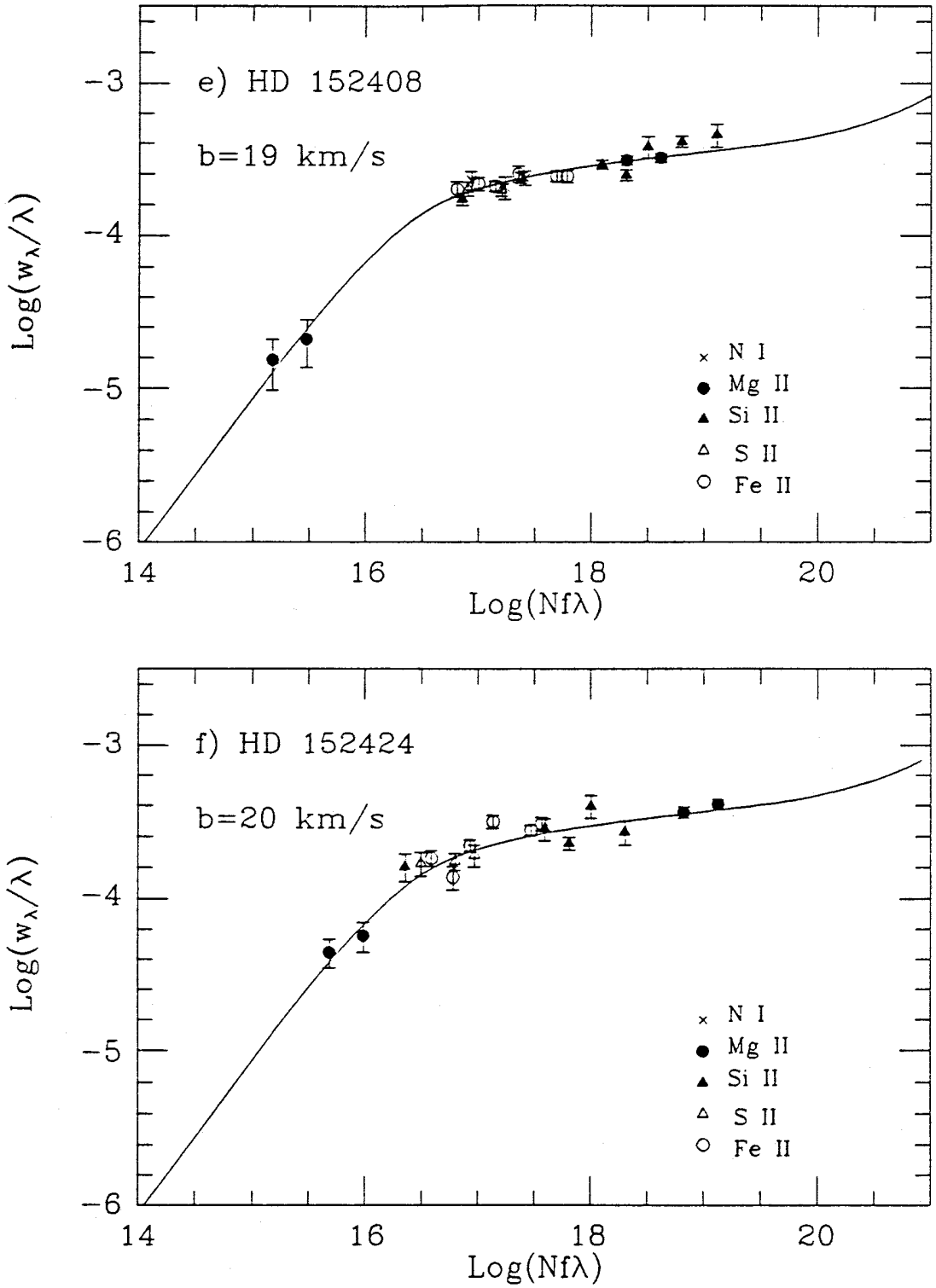

Figure 3(e,f). Empirical curves of growth for the interstellar lines towards HD 152408 and HD 152424.

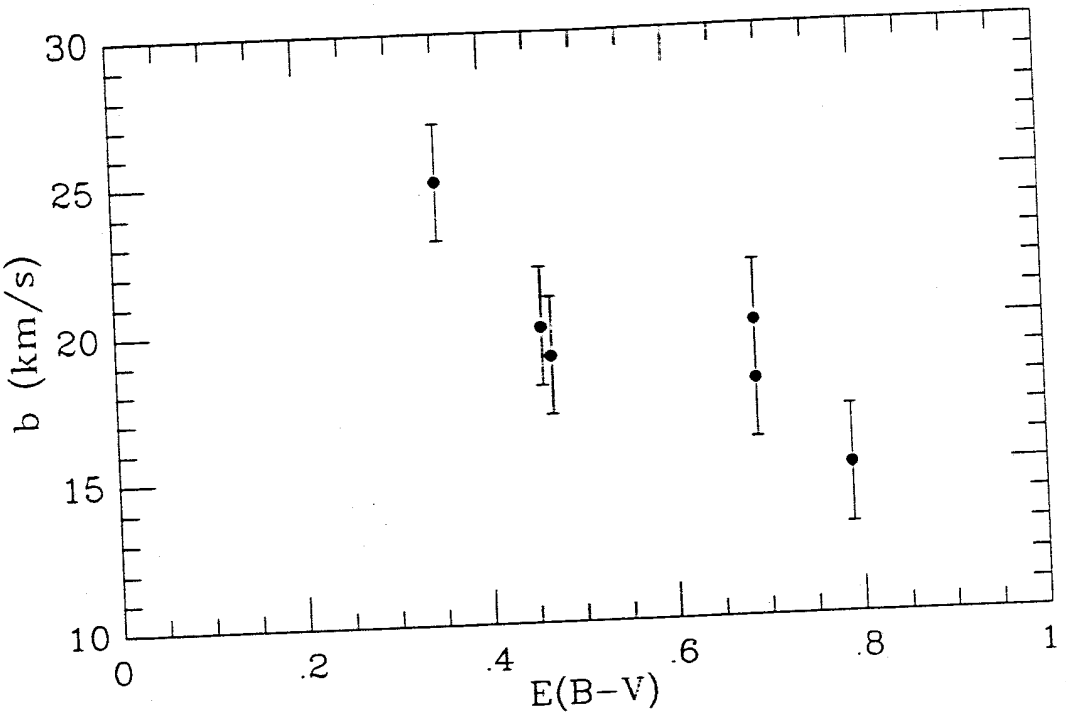

Figure 4. Observed variation of b as a function of colour excess.

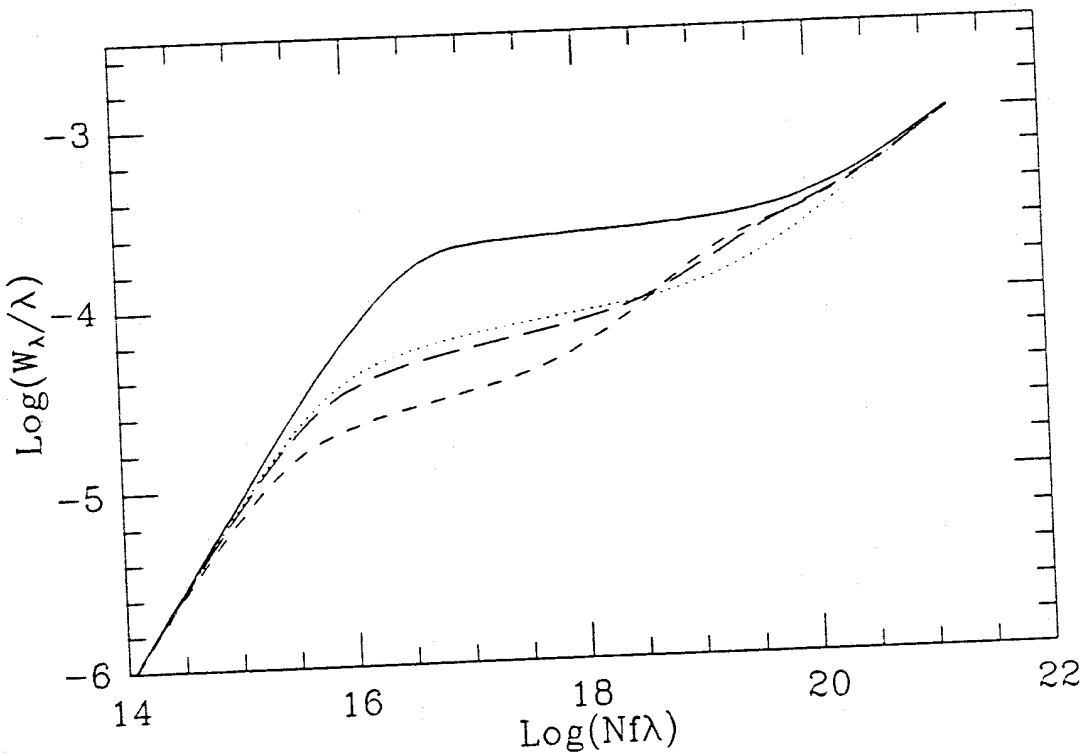

Figure 5. Some theoretical curves of growth for the 2802.7 Å line of Mg II. (a) Solid line: six clouds each with $b = 5$ km s^{-1} & $\log N = 12.5$, separated by 10 km s^{-1}; (b) short dashed line: as for (a) plus a cloud with $b = 2$ km s^{-1} & $\log N = 16.0$; (c) long dashed line: as for (a) but with two clouds each with $b = 2$ km s^{-1} & $\log N = 16.0$, separated by 10 km s^{-1}; (d) dotted line: a single cloud curve of growth with $b = 5$ km s^{-1}.

This effect is illustrated in Figure 5. The solid curve in the figure is the theoretical curve of growth (for λ2802.7, Mg II) with six components, each with b = 5 km s^{-1} and log(N) = 12.5, equally spaced at 10 km s^{-1} intervals. This is meant to represent a complex interstellar sightline with many unresolved components, such as is known to be the case for Sco OB1 from the high resolution optical observations (Crawford *et al.* 1989). The resulting curve is very similar to that due to a single component with b = 15 km s^{-1}. The short-dashed curve is the curve of growth for the same model but with an additional component with b = 2 km s^{-1} and log(N)= 16.0, which simulates the presence of a relatively dense interstellar cloud. It is clear from Figure 5 that the presence of such a cloud causes a sharp reduction in the average b value. The effect of introducing an identical cloud, displaced by 10 km s^{-1} relative to the first, is shown by the long-dashed curve. This has caused the average b value to increase, but only by a small amount compared to the initial drop. The resulting curve is very close to that which would be obtained for a single cloud with b = 5 km s^{-1} (dotted curve in the figure).

5.2 Ions with IP < 13.6 eV

It is not obvious that the remaining neutral ions (C I, Mg I, S I & Cl I) necessarily lie on the same curve of growth as the 'H I cloud' ions discussed in Section 5.1, since they could, in principle, occur predominantly in different spatial regions. If the abundances of these ions are maintained by equilibrium between photoionization and electronic recombination, we have

$$\frac{n(X^{i+1})}{n(X^i)} = \frac{\Gamma(X^i)}{\alpha(X^{i+1})n_e} \qquad (1)$$

where $n(X^i)$ and $n(X^{i+1})$ are number densities of successive ionisation stages of ion X, $\Gamma(X^i)$ is the photoionization rate for X^i, $\alpha(X^{i+1})$ is the recombination rate of X^{i+1} to X^i and n_e is the electron density. Thus it can be seen that the neutral ions would be most important in any region that happened to have a higher than average electron density. Morton (1975) used this argument together with the higher velocity resolution available with *Copernicus*) to suggest that these ions dominate in just one of the ζ Oph cloud components with a larger n_e than the others. Moreover, Morton obtained a significantly lower b value for these ions (~0.9 km s^{-1}) than for those with ionisation potentials >13.6 eV (~6.5 km s^{-1}).

In the present study none of these neutrals, with the exception of C I, were found to have sufficient lines to define an empirical curve of growth. We discuss all these ions in turn below:

1) C I. In all cases the C I lines were found to exhibit so much scatter, presumably as a result of the blends that afflict the C I spectrum (Table 2) and/or inaccurate oscillator strengths, that they did not well constrain a curve of growth. The limits that were obtained on the b values are given in Table 3 below.

Table 3.
Limits to the b value obtained from the C I lines.

star	b_{CI} (km s^{-1})
HD 151804	$4 \leq b_{CI} \leq 10$
HD 152234	$10 \leq b_{CI} \leq 16$
HD 152235	$10 \leq b_{CI}$
HD 152236	$4 \leq b_{CI} \leq 16$
HD 152408	$4 \leq b_{CI} \leq 15$
HD 152424	$7 \leq b_{CI} \leq 13$

It is apparent from Table 3 that, although the uncertainty on b for the C I lines is much larger than for the other ions, its numerical value is almost certainly smaller. This is qualitatively consistent with Morton's result for ζ Oph, and presumably indicates that the neutral carbon is significant in fewer of the unresolved velocity components.

2) Mg I. The 2852.1 Å line of Mg I was observed for all stars except HD 152235. In all cases b_{MgI} >10 km s^{-1} assuming that the line does not lie on the damping portion of the curve of growth. This would be compatible with the non-observation of damping wings in the spectra. A trial line profile calculation for the Mg I 2852Å line towards HD 151804 gave $10 \lesssim b \lesssim 30$ km s^{-1} (assuming a FWHM for the IRF of 30 km s^{-1}, Section 2).

3) S I. For HD 151804, 152234, 152236, 152408 and 152424 the S I line(s) are on the linear part of all curves of growth with $b_{SI} \geq 5$ km s^{-1}. For those stars with more than one S I line (HD 152234, HD 152424) the distribution of points on the curve of growth is not consistent with $b_{SI} < 5$ km s^{-1}, *i.e.* there is no evidence of the curve flattening out. Moreover, if we assume that S I is co-existent with Mg I, then the fact that $b_{MgI} > 10$ km s^{-1} strongly suggests that b_{SI} >5 km s^{-1}, and that these lines are indeed on the linear part. For HD 152235 the one observed line can be made to fit almost any curve of growth, but b_{SI} >5 km s^{-1} if the line does not lie on the damping part of the curve of growth.

4) Cl I. The points due to the Cl I line(s) for all six stars lie on or near the linear part of the curve of growth for all $b_{ClI} \geq 10$ km s^{-1}.

5.3 The highly ionised species

Following the discussion in Section 5.1, it is likely that the ions C IV, N V, Al III, Si III and Si IV do not exist in the same regions as the other ions, and may therefore be described by different curves of growth. Black *et al.* (1980) have discussed the occurrence of highly ionised species in the interstellar medium, based on an analysis of 11 early type stars, including two of those presently being considered (HD 151804 and HD 152424). Black *et al.* concluded that the lines of C IV, Si III and Si IV probably arise in the H II regions surrounding the stars, whereas N V may belong either to the coronal interstellar gas or arise in the interaction between the stellar winds and circumstellar material. This difference in probable origin and location of N V is due to the very large photon energy (77.5 eV) needed to produce it. However, in the present survey, only upper limits to interstellar N V were obtained. Black *et al.* do not discuss Al III, however, since the energy needed to produce it (18.8 eV) is similar to that required to produce Si III (16.3 eV), it is reasonable to suppose that they occur in the same region, namely in the H II region of the OB association.

Although Black *et al.* found that the radial velocities of the highly ionised species were similar to those of the other interstellar lines, significant blue-shifts were found in the present sample. The measured velocities are given in Table 4. Because of the small instrumental wavelength shifts ($\pm$ ~0.03Å) which appear to remain in the spectra after wavelength calibration (Section 2) the wavelength shifts for the species of interest were measured relative to neighbouring lines of the H I region ions. The measuring error was found to be about $\pm$0.04Å, which corresponds to a different velocity error at different wavelengths.

Table 4.
Observed radial velocities, relative to the other interstellar lines, of the highly ionised species observed towards Sco OB1 (km s^{-1}).

Star HD	C IV 1548Å	Al III 1855Å	Al III 1863Å	Si III 1207Å	Si IV 1394Å	Si IV 1403Å
151804	-17 ± 8	-36 ± 6	-37 ± 6	-12 ± 10	-32 ± 9	.....
152234	-4 ± 8	-11 ± 6	-10 ± 6	-15 ± 10	-30 ± 9	.....
152235	.....	-13 ± 6	-5 ± 6	.....	-32 ± 9	.....
152236	$+2 \pm 8$	-22 ± 6	-29 ± 6	.....	.....	-4 ± 9
152408	$+4 \pm 8$	-15 ± 6	-19 ± 6	-10 ± 10	-13 ± 9	-19 ± 9
152424	-2 ± 8	.....	.....	$+2 \pm 10$	-6 ± 9	-21 ± 9

It can be seen from Table 4 that there is no significant velocity displacement for the lines of C IV (except possibly for HD 151804), but that an apparently significant blue-shift of between about 10 and 30 km s^{-1} does exist for the

Al III, Si III (except HD 152424) and Si IV (except HD 152236) lines. The radial velocity of the Sco OB1 association is about -25 ± 5 km s^{-1} (*cf.* the discussion in §IV(a) of Crawford *et al.* 1989), so negative velocities of this order are consistent with an origin in the H II region local to the association. Clearly, the low velocities found for C IV are not consistent with this interpretation, and would be better understood if this ion exists in a hot ionised 'coronal' phase of the interstellar medium along the line of sight. Cowie, Taylor & York (1981) have given an expression for the expected coronal gas contribution to the C IV column density, which, for a distance of 1900 pc, predicts $\log N$(C IV) $\sim$ 13.3. This is very close to the observed C IV column densities (*cf.* Table 5, below) and supports an origin in the coronal phase. Cowie *et al.* also give expressions for the coronal contribution to the N V and Si IV column densities. These predict $\log N$(N V) = 12.9, close to the upper limits given in Table 5, and $\log N$(Si IV) = 12.1, much smaller than the observed value and consistent with the bulk of the Si IV existing in the H II region.

No correlation was found between the strengths of these lines, or their velocities, with the stellar spectral types or with the mass-loss rates given by Bertout *et al.* (1985). This is consistent with them forming in the H II region surrounding the association (or, in the case of C IV, in the interstellar coronal gas), far from the influence of the particular association member towards which they are observed.

The thermal b value for silicon at a typical H II region temperature of 10^4 K is 2.4 km s^{-1}, although the actual b value would be expected to be greater than this owing to turbulence in the H II region. In collisionally ionised gas (appropriate for the coronal phase) C IV peaks in abundance at a temperature of 1×10^5 K (see Table 2 of Savage 1987) which corresponds to a b value of 11.8 km s^{-1}. Black *et al.* (1980) claimed $7.5 \leq b \leq 20$ km s^{-1} for both C IV and Si IV towards all but two of their stars (neither of the exceptions were HD 151804 or 152424) on the basis of line profile fitting. However, because of the large width of the *IUE* instrumental response function, and its uncertainty, the present author found this method to be insensitive to adopted b values $\lesssim$15 km s^{-1}. For this reason (apart for a few exceptions noted below) a line profile analysis was not found to be particularly useful.

Only Al III (5 stars) and Si IV (2 stars) had more than one measurable line, and so only in these cases is it possible to place constraints on the curve of growth. We discuss the results for the highly ionized species from the point of view of a curve of growth analysis below.

1) C IV. The observed interstellar C IV (1548.2 Å) line would be on the linear part of a curve of growth with $b_{CIV} \gtrsim 10$ km s^{-1} for HD 152234 & HD 152408, and with $b_{CIV} \gtrsim 20$ km s^{-1} for HD 151804, HD 152236 & HD 152424. In the case of HD 151804 the C IV line was found to be very broad (FWHM$\sim$90 km s^{-1}) and easily resolved by the instrument. Theoretical line profiles indicated

$35 \lesssim b_{CIV} \lesssim 45$ km s^{-1} in this case. For the other stars the line was certainly narrower, and the same procedure yielded $b_{CIV} \lesssim 20$ km s^{-1}.

2) N V. Only upper limits were obtained for this ion. In all cases except HD 152234 these upper limits correspond to the linear part of any curve of growth with $b_{NV} \gtrsim 2$ km s^{-1}. For HD 152234, b must be $\gtrsim 5$ km s^{-1} for the linear assumption to be valid. Black *et al.* (1980) record a detection of the 1242 Å line with an equivalent width of 20mÅ towards HD 151804, which is inconsistent with the upper limit of 6 mÅ found here (Table 2).

3) Al III. The measured equivalent widths of the two lines (1854.7 Å and 1862.8 Å) was found to imply $b_{AlIII} \gtrsim 20$ km s^{-1} for HD 151804, and $b_{AlIII} \gtrsim 10$ km s^{-1} for HD 152235, HD 152236 & HD 152408. In all theses cases the lines were on or near the linear part of the curve for these b values. These lines were observed to be significantly broader than the IRF, and a line profile analysis confirmed the relatively large b values inferred from the curve of growth. For HD 152234 the observed points placed no useful limit on the b value. (The interstellar Al III lines were not measured for HD 152424 due to severe confusion with the stellar lines.)

4) Si III. The Si III (1206.5 Å) line was found to be very strong for the four stars where it was measurable (Table 2). In all four cases $b_{SiIII} \gtrsim 10$ km s^{-1} is implied unless the line lies on the damping part of the curve of growth, and the line is on the flat part for $10 \lesssim b_{SiIII} \lesssim 25$ km s^{-1}. A line profile analysis confirmed that $b_{SiIII} \gtrsim 10$ km s^{-1}, since damping wings were not present in the spectra.

5) The pair of Si IV lines (1393.8 Å and 1402.8 Å) observed towards HD 152408 and HD 152424 did not place a useful limit on b_{SiIV}. We note only that these points are on the linear part for $b_{SiIV} \gtrsim 5$ km s^{-1}. For the other stars, each with only one measured Si IV line, the line is on the linear part for $b_{SiIV} \gtrsim 10$ km s^{-1}.

6 Ionic abundances and atomic depletions

The column densities for those species used to define the curve of growth (N I, Mg II, Si II, S II and Fe II) and those assumed to spatially co-existent with them (C II, O I, Al II, Mn II, Ni II, Cu II and Zn II) can be obtained directly from the empirical curves of growth. The procedure adopted was to apply a linear horizontal shift of magnitude $\log(N)$, where N is the desired column density, for each line such that it lay on the appropriate theoretical curve of growth, with empirically determined b. For very strong lines it was necessary to construct individual theoretical curves because the damping parts of curves of growth are in general different for different lines.

Errors on the column density for each line were obtained from the equivalent width error bars *and* the empirically determined error on b of $\pm$ 2 km s^{-1}. The uncertainty in b only affects lines on or near the flat part of the curve of growth, although in practice this includes most of them. For such lines the upper limit to log(N) was obtained from the shift necessary to fit the upper w_λ error bar to the theoretical curve with the minimum allowed b value, and *vice versa*. Once column densities had been obtained from each line of a given ion, the column density of the ion itself was obtained by performing a weighted mean of the results from the individual lines. Since the errors obtained from each line are generally asymmetric, it was decided to weight by the range of log(N) for each line and then maintain the same degree of asymmetry on the resulting error on the mean.

Because of the uncertainties inherent in the curve of growth analysis for the remaining neutral and highly ionised species, the determination of their column densities is not so straightforward. If we assume that all the ions with ionisation potentials <13.6 eV arise predominantly in the same regions along the line of sight, then the evidence from the S I and Mg I lines (Section 5.2) sets a lower limit to the appropriate velocity dispersion of $b \gtrsim 10$ km s^{-1}. This is consistent with the ranges determined from the C I lines (Table 3) for all stars except possibly HD 151804. This conclusion immediately implies that the lines of S I and Cl I are on or near the linear part of the curve of growth, and hence the errors on their column densities result from the errors in the equivalent width measurements only.

For C I and Mg I it was decided to adopt a lower limit of 10 km s^{-1} to the b value and an upper limit equal to the maximum allowed by the C I lines (Table 3). For HD 151804, for which the maximum b_{CI} value was also 10 km s^{-1}, errors of $\pm$ 3 km s^{-1} were arbitarily assumed. For HD 152235, for which the C I curve of growth did not provide an upper limit to b, a maximum value of 16 km s^{-1} was assumed. This is thought to be conservative since 16 km s^{-1} is the largest upper limit to b_{CI} found for the other stars (Table 3).

The ionic column densities obtained from the curve of growth analysis are given in Table 5. The number of lines used for each determination is also indicated.

Before the ionic column densities given in Table 5 can be used to calculate the elemental depletions, it is necessary to determine the hydrogen column density towards each star. H I column densities, derived by profile fitting to the interstellar Lyα line, have been given for HD 151804, 152234, 152236 and 152408 by Shull & Van Steenberg (1985). For HD 152235 and HD 152424 the merged *IUE* spectra used in this study were found to be insufficiently exposed in the region of Lyα to permit the author to determine N(H I) by the same method, and use was made of the the empirical relation given by Bohlin, Savage & Drake (1978):

$$N(\text{H I})/E_{B-V} = 4.8 \times 10^{21} \text{cm}^{-2}\text{mag}^{-1}. \qquad (2)$$

Table 5.

The logarithms of the ionic column densities towards the Sco OB1 association. The numbers in parentheses give the number of lines used to obtain the weighted mean for the column density of each ion. (Units are cm^{-2}.)

Ion	151804	152234	152235	152236	152408	152424
C I	$14.51^{+0.40}_{-0.14}(6)$	$14.32^{+0.14}_{-0.13}(5)$	$13.52^{+0.20}_{-0.18}(2)$	$14.22^{+0.32}_{-0.14}(4)$	$14.18^{+0.19}_{-0.13}(8)$	$14.38^{+0.09}_{-0.09}(5)$
C I*	$13.56^{+0.21}_{-0.23}(3)$	$14.30^{+0.17}_{-0.12}(4)$	$13.97^{+0.20}_{-0.14}(2)$	$14.29^{+0.21}_{-0.16}(4)$	$13.89^{+0.15}_{-0.12}(3)$	$14.25^{+0.11}_{-0.12}(5)$
C I**	$\lesssim$12.9 (2)	$13.88^{+0.14}_{-0.12}(3)$	$13.70^{+0.13}_{-0.13}(2)$	$14.00^{+0.23}_{-0.15}(2)$	$13.94^{+0.11}_{-0.11}(3)$	$13.86^{+0.12}_{-0.11}(3)$
C II	$16.50^{+0.70}_{-0.70}(1)$	$17.25^{+0.50}_{-0.50}(1)$	...	...	$16.80^{+0.95}_{-0.80}(1)$	$17.70^{+0.55}_{-0.95}(1)$
C II*	$15.40^{+0.50}_{-0.30}(1)$	$15.90^{+1.10}_{-0.65}(1)$	$17.20^{+0.85}_{-1.30}(1)$	$15.50^{+1.00}_{-0.60}(1)$	$16.25^{+1.05}_{-0.65}(1)$	$16.05^{+0.95}_{-0.65}(1)$
C IV	$13.68^{+0.12}_{-0.13}(1)$	$13.60^{+0.35}_{-0.50}(1)$	...	$13.70^{+0.17}_{-0.13}(1)$	$13.00^{+0.25}_{-0.50}(1)$	$13.45^{+0.18}_{-0.20}(1)$
N I	$14.75^{+0.45}_{-0.25}(1)$	$14.86^{+0.13}_{-0.12}(3)$	...	...	$15.21^{+0.48}_{-0.23}(3)$	...
N V	$\lesssim$12.76 (1)	$\lesssim$13.4 (1)	...	$\lesssim$12.89 (1)	$\lesssim$12.95 (1)	$\lesssim$12.60 (1)
O I	$15.95^{+0.55}_{-0.45}(1)$	$18.07^{+0.15}_{-0.15}(2)$	$18.80^{+0.40}_{-1.50}(1)$	...	$17.20^{+1.00}_{-0.90}(1)$	$16.80^{+1.10}_{-0.80}(1)$
O I*	$\lesssim$12.75 (1)	$\lesssim$13.20 (1)	$13.57^{+0.14}_{-0.21}(1)$	...	$\lesssim$13.10 (1)	$13.28^{+0.17}_{-0.28}(1)$
O I**	$13.25^{+0.15}_{-0.15}(1)$	$\lesssim$13.20 (1)	$\lesssim$13.46 (1)	$\lesssim$13.60 (1)	...	$13.32^{+0.11}_{-0.14}(1)$
Mg I	$15.00^{+0.70}_{-1.40}(1)$	$15.00^{+0.80}_{-1.10}(1)$	...	$14.70^{+0.90}_{-1.00}(1)$	$15.25^{+0.55}_{-1.05}(1)$	$15.10^{+0.50}_{-0.80}(1)$
Mg II	$15.60^{+0.10}_{-0.15}(4)$	$16.02^{+0.10}_{-0.10}(4)$	$17.00^{+0.40}_{-0.90}(1)$	$15.88^{+0.11}_{-0.11}(4)$	$15.40^{+0.11}_{-0.12}(4)$	$15.91^{+0.08}_{-0.09}(4)$
Al II	$14.15^{+0.55}_{-0.40}(1)$	$14.40^{+0.70}_{-0.60}(1)$	$15.15^{+0.55}_{-0.75}(1)$	$14.40^{+0.90}_{-0.70}(1)$	$14.80^{+0.90}_{-0.80}(1)$	$14.70^{+0.80}_{-0.70}(1)$
Al III	$13.40^{+0.07}_{-0.07}(2)$	$13.38^{+0.09}_{-0.07}(2)$	$13.34^{+0.17}_{-0.12}(2)$	$12.93^{+0.13}_{-0.16}(2)$	$13.19^{+0.08}_{-0.06}(2)$	...

Table 5(continued)

Ion	151804	152234	152235	152236	152408	152424
Si II	$15.43^{+0.08}_{-0.11}(6)$	$15.78^{+0.16}_{-0.14}(5)$	$15.96^{+0.56}_{-0.38}(3)$	$15.97^{+0.27}_{-0.21}(4)$	$16.03^{+0.18}_{-0.14}(6)$	$15.53^{+0.26}_{-0.18}(5)$
Si III	$14.40^{+0.60}_{-0.50}(1)$	$14.20^{+1.20}_{-0.60}(1)$	...	...	$15.15^{+0.60}_{-0.75}(1)$	$14.00^{+1.30}_{-0.80}(1)$
Si IV	$12.75^{+0.10}_{-0.10}(1)$	$12.55^{+0.15}_{-0.20}(1)$	$12.92^{+0.16}_{-0.17}(1)$	$12.85^{+0.25}_{-0.50}(1)$	$12.56^{+0.09}_{-0.13}(2)$	$12.70^{+0.09}_{-0.12}(2)$
S I	$13.55^{+0.08}_{-0.09}(2)$	$13.22^{+0.06}_{-0.07}(3)$	$13.78^{+0.37}_{-0.43}(1)$	$13.30^{+0.15}_{-0.25}(1)$	$12.85^{+0.15}_{-0.25}(1)$	$13.09^{+0.06}_{-0.08}(3)$
S II	$15.60^{+0.06}_{-0.06}(3)$	$15.89^{+0.25}_{-0.15}(3)$	$16.08^{+0.56}_{-0.32}(3)$	$16.42^{+0.48}_{-0.33}(2)$	$16.08^{+0.33}_{-0.21}(3)$	$15.67^{+0.25}_{-0.13}(3)$
Cl I	$13.55^{+0.09}_{-0.13}(2)$	$13.88^{+0.06}_{-0.08}(2)$	$13.40^{+0.15}_{-0.18}(1)$	$13.83^{+0.12}_{-0.15}(1)$	$13.77^{+0.11}_{-0.09}(2)$	$13.75^{+0.10}_{-0.07}(1)$
Cr II	$13.13^{+0.04}_{-0.04}(1)$	...	...	$13.25^{+0.10}_{-0.15}(1)$	$13.10^{+0.05}_{-0.05}(1)$	$12.87^{+0.06}_{-0.05}(1)$
Mn II	$13.52^{+0.05}_{-0.04}(4)$	$13.68^{+0.09}_{-0.07}(4)$	$13.84^{+0.28}_{-0.13}(4)$	$13.68^{+0.08}_{-0.06}(4)$	$13.65^{+0.08}_{-0.06}(3)$	$13.68^{+0.07}_{-0.06}(4)$
Fe II	$14.59^{+0.14}_{-0.09}(5)$	$14.63^{+0.20}_{-0.12}(6)$	$15.54^{+0.42}_{-0.34}(6)$	$14.84^{+0.24}_{-0.15}(6)$	$14.81^{+0.23}_{-0.14}(6)$	$14.59^{+0.18}_{-0.19}(6)$
Ni II	$13.60^{+0.05}_{-0.05}(1)$	$13.55^{+0.10}_{-0.10}(1)$	$13.60^{+0.18}_{-0.20}(1)$	$13.73^{+0.07}_{-0.08}(1)$	$13.72^{+0.13}_{-0.12}(1)$	$13.58^{+0.12}_{-0.10}(1)$
Cu II	...	$12.22^{+0.13}_{-0.17}(1)$	...	...	...	$12.62^{+0.18}_{-0.30}(1)$
Zn II	$13.43^{+0.11}_{-0.13}(1)$	$13.95^{+0.45}_{-0.25}(1)$	$\lesssim 16.50$ (1)	$13.35^{+0.10}_{-0.15}(1)$	$13.81^{+0.14}_{-0.11}(1)$	$14.03^{+0.57}_{-0.33}(1)$

Bohlin, Savage & Drake give measured H_2 column densities, based on *Copernicus* observations, for HD 151804 and HD 152408. For all other stars their empirical relation,

$$N(H_2)/E_{B-V} = 5.0 \times 10^{20} \mathrm{cm}^{-2}\mathrm{mag}^{-1}, \tag{3}$$

was used. Note that $N(H_2)$ found from these relations is about 10% of N(H I), so the errors in the total hydrogen column density due to using an empirical relation for $N(H_2)$ for stars that have directly measured N(H I) is very small. For HD 152235 and HD 152424 there are no direct observations of either H I or H_2 available, and it was necessary to use the empirical relation of Bohlin, Savage & Drake for the total column density of hydrogen nuclei:

$$N(\mathrm{H\ I} + H_2)/E_{B-V} = 5.8 \times 10^{21}\ \mathrm{cm}^{-2}\mathrm{mag}^{-1}, \tag{4}$$

where N(H I + H_2) $\equiv N$(H I) + $2N(H_2)$.

The total hydrogen column densities obtained in this way are given in Table 6. Shull & Van Steenberg quote errors of about 20% on their N(H I) determinations for the stars in question. Bohlin, Savage & Drake note that, for the stars in their survey, measured N(H I + H_2) values are generally within a factor of 1.5 of the mean value given by their empirical relation. However, for the two members of Sco OB1 with measured values (HD 151804 and HD 152408) the agreement is considerably better than this. In both cases the empirical relation produced values that differed by about 20% from the observed column densities, in the sense that the empirical relation overestimated the total column density. This agreement gives one hope that the total hydrogen column densities for HD 152235 and HD 152424, for which only the empirical relation was used, also have an error no worse than about 20%.

Table 6.
Total hydrogen column densities for the Sco OB1 stars. The uncertainty on these values is about 20%. Units are cm^{-2}.

Star	log N(H I + H_2)	Star	log N(H I + H_2)
151804	21.21	152236	21.79
152234	21.34	152408	21.31
152235	21.66	152424	21.60

The depletion factor, δ_X, of element X is defined by:

$$\delta_X = \log[N(\mathrm{X})/N(\mathrm{H})] - \log[N(\mathrm{X})/N(\mathrm{H})]_\odot \qquad (5)$$

where $N(X)$ is the column density of element X, $N(\mathrm{H})$ is the column density of hydrogen (H I + H_2) and $[N(X)/N(H)]_\odot$ is the ratio of X to hydrogen in the sun.

The cosmic abundances of the elements used to calculate the depletions were taken from Grevesse (1984, quoted by Cowie & Songaila 1986) and are the averages of solar and meteoritic values, except for C, N and O, which are solar values only. They are reproduced in Table 7 below.

Table 7.
Cosmic abundances of the elements relative to
log $N(\mathrm{H}) = 12$. Taken from Grevesse (1984).

Atom	Abund.	Atom	Abund.	Atom	Abund.
H	12.00	Si	7.55	Mn	5.49
C	8.69	S	7.24	Fe	7.59
N	7.99	Cl	5.40	Co	4.92
O	8.91	K	5.13	Ni	6.25
Na	6.32	Ca	6.35	Cu	4.23
Mg	7.58	Cr	5.67	Zn	4.63
Al	6.48				

Most of the above elements have been observed in all the ionisation stages likely to be important in the neutral interstellar medium, and so the total column density can be obtained by adding the column densities of these different stages. The depletion factors, δ_X, obtained from the information given in Tables 5, 6 and 7, assuming an error of 20% in the hydrogen column densities but no error in the solar abundances, are given in Table 8 and are shown graphically in Figure 6. The lower limits shown for C towards HD 152235 and HD 152236 are due to the non-detection of the C II line and are based on C II* only. The lower limits for the Na and Ca depletions towards HD 152235 result from the inability to estimate the relative abundance of the higher ionisation stages, owing to the non-detection of the Mg I line in this star (see below). The lower limits are therefore based on Na I and Ca II only.

Table 8.

Logarithmic element depletions towards Sco OB1. The ionisation states included for each ion are indicated in the first column.

Atom	151804	152234	152235	152236	152408	152424
C (II+II*)	$-1.37^{+0.79}_{-0.73}$	$-0.76^{+0.65}_{-0.60}$	$\gtrsim -2.53$	$\gtrsim -3.66$	$-1.09^{+1.07}_{-0.84}$	$-0.58^{+0.66}_{-1.02}$
N (I)	$-2.45^{+0.55}_{-0.33}$	$-2.47^{+0.23}_{-0.20}$	...	...	$-2.09^{+0.58}_{-0.31}$	...
O (I)	$-2.17^{+0.65}_{-0.53}$	$-0.18^{+0.25}_{-0.23}$	$+0.23^{+0.50}_{-1.58}$	...	$-1.02^{+1.10}_{-0.98}$	$-1.71^{+1.20}_{-0.88}$
Na (I+II)	$-1.19^{+2.10}_{-1.25}$	$-0.63^{+1.60}_{-1.13}$	$\gtrsim -2.52$	$-0.26^{+1.45}_{-1.88}$	$-1.12^{+1.57}_{-1.00}$	$-0.66^{+1.78}_{-1.33}$
Mg (I+II)	$-1.09^{+0.40}_{-0.32}$	$-0.86^{+0.33}_{-0.22}$	$-0.24^{+0.50}_{-0.98}$	$-1.46^{+0.33}_{-0.21}$	$-1.26^{+0.45}_{-0.40}$	$-1.21^{+0.27}_{-0.22}$
Al (II+III)	$-1.47^{+0.61}_{-0.41}$	$-1.38^{+0.77}_{-0.60}$	$-0.98^{+0.63}_{-0.81}$	$-1.85^{+0.98}_{-0.75}$	$-0.98^{+0.99}_{-0.84}$	$-1.38^{+0.90}_{-0.78}$
Si (II+III)	$-1.29^{+0.26}_{-0.21}$	$-1.10^{+0.36}_{-0.23}$	$-1.25^{+0.66}_{-0.46}$	$-1.37^{+0.37}_{-0.29}$	$-0.78^{+0.36}_{-0.26}$	$-1.61^{+0.47}_{-0.27}$
S (II)	$-0.85^{+0.16}_{-0.14}$	$-0.69^{+0.35}_{-0.23}$	$-0.82^{+0.66}_{-0.40}$	$-0.61^{+0.58}_{-0.41}$	$-0.47^{+0.43}_{-0.29}$	$-1.17^{+0.35}_{-0.21}$
Cl (I+II)	$-0.39^{+1.59}_{-0.70}$	$+0.17^{+1.31}_{-0.84}$	$\gtrsim -1.92$	$-0.18^{+1.30}_{-1.03}$	$-0.57^{+1.15}_{-0.43}$	$-0.40^{+1.02}_{-0.59}$
Ca (II+III)	$-2.71^{+0.61}_{-0.16}$	$-2.75^{+0.65}_{-0.20}$	$\gtrsim -3.27$	$-3.14^{+0.70}_{-0.21}$	$-2.73^{+0.26}_{-0.20}$	$-3.07^{+0.38}_{-0.18}$
Cr (II)	$-1.70^{+0.14}_{-0.12}$	...	...	$-2.21^{+0.20}_{-0.23}$	$-1.88^{+0.15}_{-0.13}$	$-2.40^{+0.16}_{-0.13}$
Mn (II)	$-1.18^{+0.15}_{-0.12}$	$-1.15^{+0.19}_{-0.15}$	$-1.31^{+0.38}_{-0.21}$	$-1.60^{+0.18}_{-0.14}$	$-1.15^{+0.18}_{-0.14}$	$-1.41^{+0.17}_{-0.14}$
Fe (II)	$-2.21^{+0.24}_{-0.17}$	$-2.30^{+0.30}_{-0.20}$	$-1.71^{+0.52}_{-0.42}$	$-2.54^{+0.34}_{-0.23}$	$-2.09^{+0.33}_{-0.22}$	$-2.60^{+0.28}_{-0.27}$
Ni (II)	$-1.86^{+0.15}_{-0.13}$	$-2.04^{+0.20}_{-0.18}$	$-2.31^{+0.28}_{-0.28}$	$-2.31^{+0.17}_{-0.16}$	$-1.84^{+0.23}_{-0.20}$	$-2.27^{+0.22}_{-0.18}$
Cu (II)	...	$-1.35^{+0.23}_{-0.25}$	$\lesssim +1.29$	$\lesssim +1.14$	...	$-1.21^{+0.28}_{-0.38}$
Zn (II)	$-0.41^{+0.21}_{-0.21}$	$-0.02^{+0.55}_{-0.33}$	$\lesssim +2.31$	$-1.07^{+0.20}_{-0.23}$	$-0.13^{+0.24}_{-0.19}$	$-0.20^{+0.67}_{-0.41}$

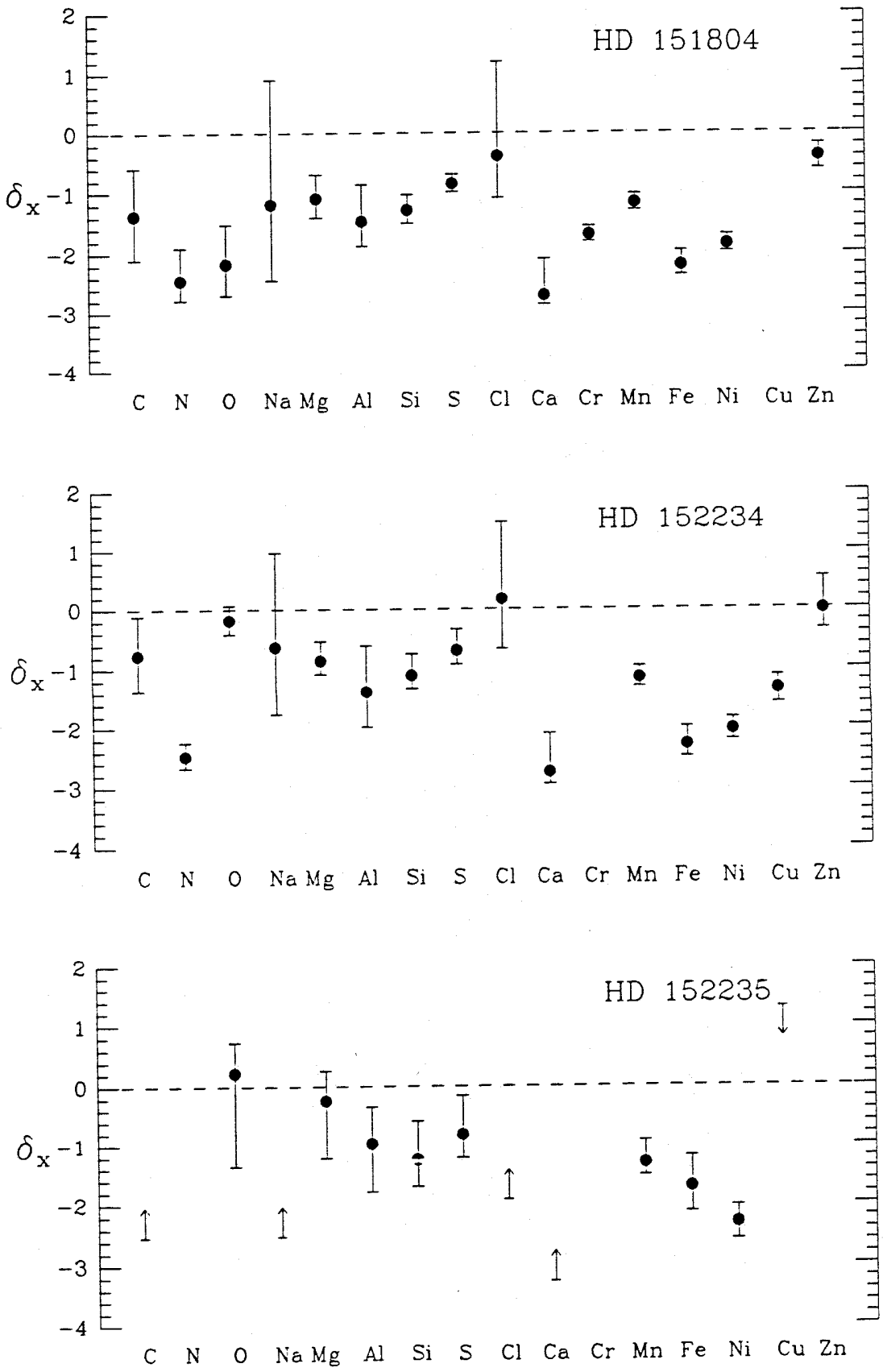

Figure 6. Interstellar atomic depletions determined for the Sco OB1 sightlines.

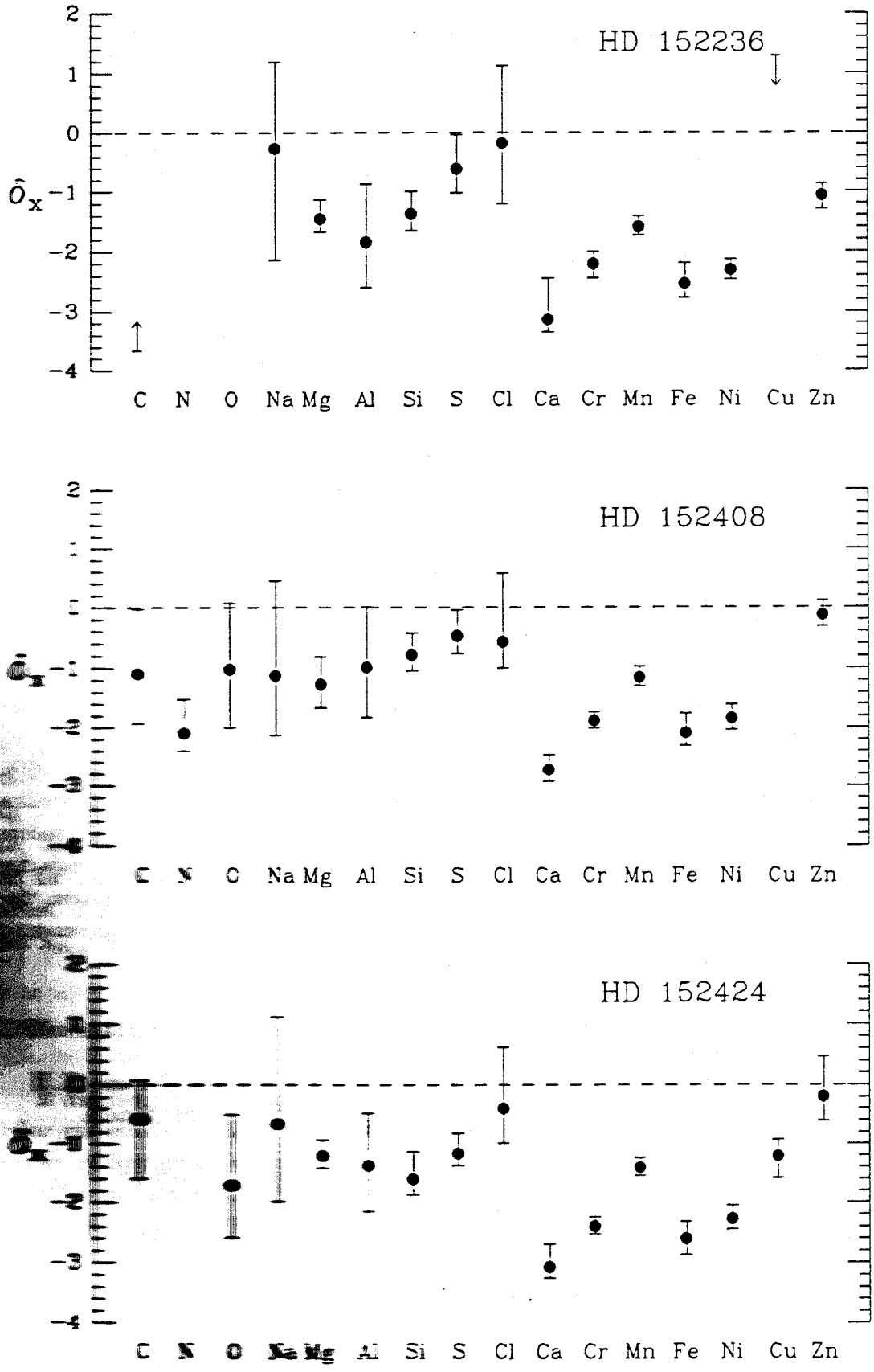

Figure 6 (continued). Interstellar atomic depletions determined for the Sco OB1 sightlines.

6.1. The depletions of Na, Ca & Cl

Because of their low ionisation potentials, the ions Na I, Ca II and Cl I are not usually the dominant ionisation states of these atoms under interstellar conditions. In fact, Na I and Ca II are generally considered to be only minor ionisation stages, and lines of the dominant stages (Na II & Ca III) are not observable. A line of Cl II (1071 Å) was observable with *Copernicus*, but is well outside the wavelength coverage of *IUE*.

It is necessary to estimate the column densities of the unobserved ionisation stages. Here we have followed Phillips, Pettini & Gondhalekar (1984) and rearranged the photoionisation – recombination relation (Equation 1) to give:

$$\frac{n(\mathrm{NaII})}{n(\mathrm{NaI})} = \frac{n(\mathrm{MgII})}{n(\mathrm{MgI})} \times \frac{\Gamma(\mathrm{NaI})}{\Gamma(\mathrm{MgI})} \times \frac{\alpha(\mathrm{MgII})}{\alpha(\mathrm{NaII})}. \qquad (6)$$

The explicit dependence on n_e has cancelled out of this expression. If it is assumed that the space distributions of these ions correspond (probably not the case, see below) then the space densities can be equated with the observed column densities. The observed Mg I/Mg II ratio has been used to eliminate the electron density from the expression. Similar expressions hold for the Ca III/Ca II and Cl II/Cl I ratios.

Taking the Na I and Ca II column densitiies from Crawford *et al.* (1989), the photoionisation rates, Γ, from Keenan (1984), which assume the interstellar radiation field of Gondhalekar, Phillips & Wilson (1980), and the recombination rates, α (for $T = 100$ K), from Aldrovandi & Péquignot (1973, 1974), yields the Na II, Ca III & Cl II column densities given in Table 9. For comparison, the column densities of Na I, Ca II (summed over all resolved velocity components) and Cl I are also given.

Table 9.

Logarithmic column densities of Na I, Na II, Ca II, Ca III, Cl I and Cl II towards the Sco OB1 stars. Units are cm^{-2}. See text for details.

Star	N(Na I)	N(Na II)	N(Ca II)	N(Ca III)	N(Cl I)	N(Cl II)
151804	$13.92^{+0.70}_{-0.84}$	$14.13^{+2.20}_{-1.69}$	$12.83^{+0.08}_{-0.06}$	$11.58^{+1.58}_{-0.91}$	$13.55^{+0.09}_{-0.13}$	$14.12^{+1.59}_{-0.98}$
152234	$14.31^{+0.39}_{-0.52}$	$14.94^{+1.59}_{-1.42}$	$12.88^{+0.09}_{-0.07}$	$12.05^{+1.29}_{-0.97}$	$13.88^{+0.06}_{-0.08}$	$14.87^{+1.26}_{-0.98}$
152235	$14.71^{+0.61}_{-1.17}$	...	$12.85^{+0.10}_{-0.03}$	...	$13.40^{+0.15}_{-0.18}$	...
152236	$15.00^{+0.30}_{-1.15}$	$15.78^{+1.41}_{-2.16}$	$12.92^{+0.11}_{-0.05}$	$12.25^{+1.22}_{-1.06}$	$13.83^{+0.12}_{-0.15}$	$14.98^{+1.23}_{-1.16}$
152408	$14.31^{+0.70}_{-0.77}$	$14.07^{+1.86}_{-1.44}$	$12.92^{+0.06}_{-0.11}$	$11.22^{+1.22}_{-0.78}$	$13.77^{+0.11}_{-0.09}$	$13.89^{+1.27}_{-0.76}$
152424	$14.70^{+0.92}_{-0.91}$	$15.12^{+1.80}_{-1.50}$	$12.84^{+0.09}_{-0.07}$	$11.80^{+0.97}_{-0.66}$	$13.75^{+0.10}_{-0.07}$	$14.53^{+0.98}_{-0.66}$

These are the ionic column densities used for the depletions of Na, Ca and Cl given in Table 8 and Figure 6. The large errors quoted on the column densities for the higher ionisation stages reflect the uncertainty in the Mg I and Mg II column densities used in the calculation.

Inspection of Table 9 shows that, far from Na I and Ca II being trace ionisation stages, the column density of Na I is comparable (*i.e.* the same order of magnitude) to that of Na II, and the Ca II column density dominates that of Ca III. This is a direct consequence of the large Mg I column densities determined from the curve of growth analysis which, from Equation 6, leads to relatively low column densities for the higher ionisation stages. Physically, a large N(Mg I) implies large n_e, which leads to a large population in the lower ionisation stages because of recombination. However, we noted in Section 5.2 that the neutral ions with ionisation potentials $\leq$13.6 eV may arise in different spatial regions (with higher n_e) from the other ions. This was supported by the lower b value for the curves of growth of these ions. Thus the assumption that the Mg I lines arise from the same regions as the Mg II lines, implicit in Equation 6, is probably incorrect. Clearly, the effect of this assumption will be to overestimate n_e in the regions containing Mg II, Na II, Ca III and Cl II, with the consequent underestimation of the column density of the latter three ions. Only the advent of very high spectral resolution in the UV, enabling the determination of n_e in each velocity component, will resolve this difficulty.

Finally, we note that if we use the same curves of growth to determine N(Mg I) as were used for N(Mg II) (out of keeping with the results for the other neutrals, but not ruled out by the Mg I observations themselves) the Mg I column density would be reduced, and the resulting depletion reduced (*i.e.* the elements become *less* depleted) by about 1.0–1.5 dex for Na, 0.5–1.0 dex for Ca, and 1–2 dex for Cl. This latter result would push δ_{Cl} to positive values. Since this is unlikely, this is another argument in support of the view that $b_{MgI} < b_{MgII}$.

6.2 Discussion of the atomic depletions

It has long been recognized that most elements are depleted in the interstellar gas relative to their solar (or 'cosmic') abundances (see, for example, the reviews by Spitzer & Jenkins 1975 and Cowie & Songaila 1986). It is known that molecules are not sufficiently abundant to account for this depletion, and so it is generally accepted that the missing atoms are contained in, or on, interstellar grains.

Most of the depletions found here are consistent with the general pattern that has emerged over the last decade, as represented, for example, by the 'average' depletions quoted by Cowie & Songaila (1986). In keeping with these previous results, S and Zn were found to be the lightly depleted. Although there does seem to be evidence for a small but significant depletion of S, three of the five stars for which a Zn abundance was measured showed a value consistent with

zero depletion. (The apparently anomalous Zn depletion towards HD 152236 should probably not be taken too seriously; as for all the stars, it is based on a single line in a noisy part of the spectrum.) Ca was found to have have the largest depletion, also in keeping with previous results, with the observed values lying well within the 'average' range given by Cowie & Songaila.

The most significant departure of the present results from previous ones is the large depletion of N found in the present case. In his detailed studies of ζ Oph and ζ Pup Morton (1975, 1978) found $-1 < \delta_N < 0$, and Cowie & Songaila (1986) quote a cononical value of $\delta_N = -0.09 \pm 0.40$. In contrast, the N depletion factors shown in Figure 6, for the three stars towards which it was measured, are about two orders of magnitudes larger than this. Note that although Hibbert *et al.* (1985) have recently revised the oscillator strengths for the N I lines, their values differ by only about 4% from those given in Table 2. However, all three N I lines are in the blue wing of interstellar Lyα (*cf.* Table 2) and are also interfered with by the stellar wind Si III (1206.5 Å) line. The most probable reason for the low N abundances, therefore, is an underestimation of the true continuum level. Because of the saturated nature of these lines (*cf.* Figure 3) an underestimate of the equivalent width by 50 % would underestimate the column density by almost an order of magnitude.

Field (1974), in a study of depletions towards ζ Oph, demonstrated a correlation between depletion and condensation temperature which he interpreted to imply that the observed (*i.e.* present day) depletions reflect the grain formation process. Subsequently it has been demonstrated by many authors (*e.g.* Phillips, Gondhalekar & Pettini 1982a,b; Phillips, Pettini & Gondhalekar 1984; Jenkins, Savage & Spitzer 1986) that the depletions of many elements correlate with the average hydrogen density, $< n_H >= N(\mathrm{H})/d$, where d is the stellar distance. This result is interpreted to mean that, although Field's view may still be partially correct, present day gas densities in the interstellar medium do effect the depletions. The most likely reason for this is accretion of gas phase atoms onto grain surfaces, since the accretion rate is proportional to density. Since the stars observed in this study are all at essentially the same distance and, therefore, differences in hydrogen column density must be due to the inhomogeneous nature of the foreground material, it was considered worthwhile to see if this effect was apparent in the present data.

Note that even for stars at the same distance, $< n_H >$ is a reliable guide to the local space density, n_H, only if there is one absorbing cloud along the line of sight. For example, consider two sightlines of the same length, one with one cloud and the other with two. If the clouds have the same size and density, $< n_H >$ will clearly be larger in the latter case because of the greater total column density, even though n_H is the same in both clouds. However, Spitzer (1985) has shown that, for sightlines which pass through more than one cloud, $< n_H >$ is a measure of the relative importance of the intercloud medium, 'standard' diffuse clouds and denser diffuse clouds along the sightline. A larger

$< n_H >$ indicates that the denser clouds contribute relatively more material to the total column density. Thus, even for multiple component sightlines, a decrease in δ_X with $< n_H >$ may still reflect greater gas-phase depletion in the denser clouds.

Although the Sco OB1 stars only exhibit a relatively small variation in $< n_H >$ (a factor of five, compared with the two orders of magnitude in the study of Phillips *et al.* 1982a, for example) apparently significant variations of δ_X with $< n_H >$ were found for the elements Ca, Cr, Mn and Ni. Figure 7 shows the depletion factors for these elements plotted against $< n_H >$. The assumed distance was 1900 pc and the hydrogen column densities were taken from Table 6. Also shown are the gradients found by performing a weighted least squares fit to each set of data. These gradients are consistent with the results of Phillips *et al.* (1982a,b, 1984), who found values of -1.22 ± 0.18, -0.52 (with no error quoted), -0.41 ± 0.09 and -0.61 ± 0.13 for Ca, Cr, Mn and Ni respectively. The depletions for all other elements were found to be consistent with no dependence on $< n_H >$, although the errors bars on some of them (particularly Al, for which Phillips *et al.* 1982a found a strong dependence) are such that a trend might still be consistent with the data.

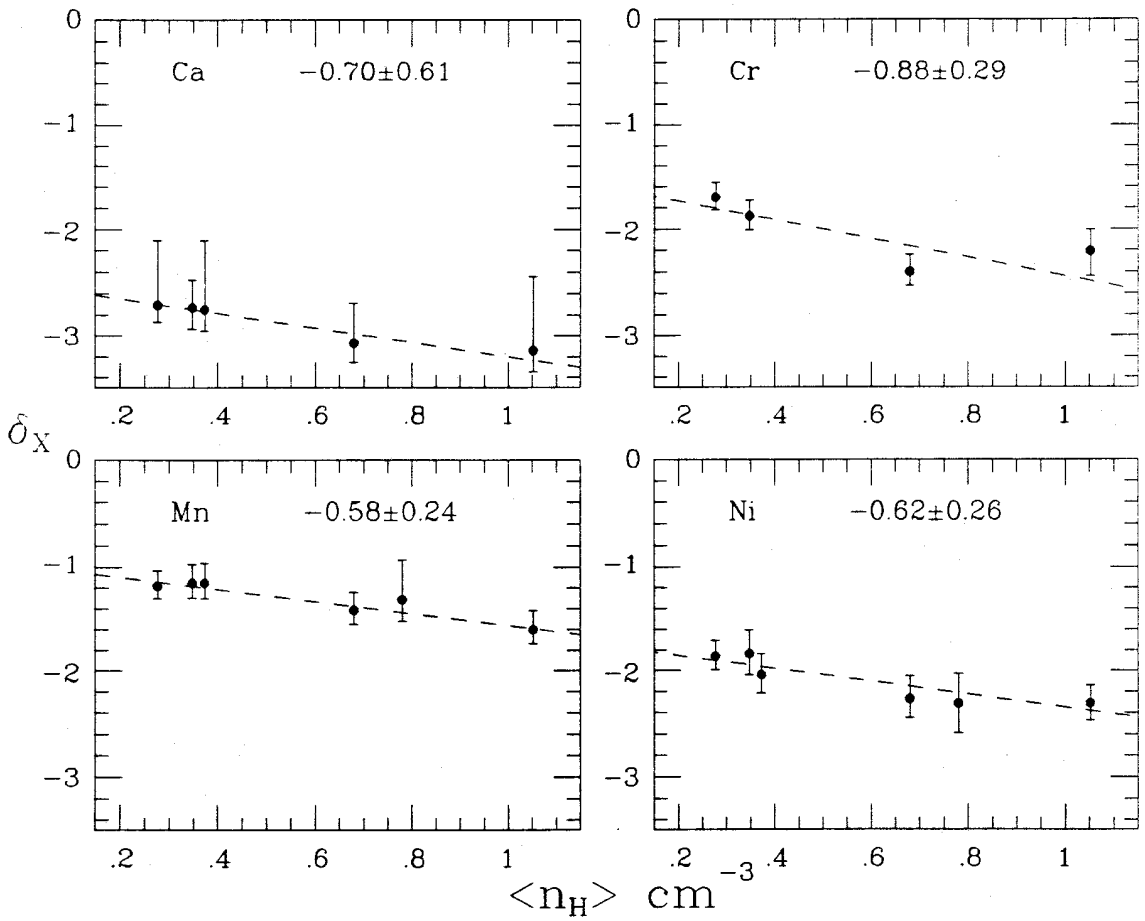

Figure 7. Depletion factors plotted against the mean line-of-sight hydrogen density, $< n_H >$, for the elements Ca, Cr, Mn & Ni. The dashed lines are weighted least square fits to the points. The gradients found for these lines are indicated in each box. See text for discussion.

7 Physical conditions derived from the UV data

7.1 The mean electron densities

Equation 1 can be used to estimate the average electron density, $< n_e >$, from the observed column densities of successive ionisation states of the same atom. It is necessary to assume that the column densities can be equated with the space densities, which is the same as assuming that both ionisation states exist predominantly in the same spatial regions. As discussed at length in Section 6.1, there is some evidence that this is not the case, which means that these electron densities cannot be interpreted too literally. It is, nevertheless, of interest to compare the values of $< n_e >$ obtained from different atoms.

From the present study it was possible to obtain values of $< n_e >$ from the ratios of neutral and singly ionised C, Mg and S. The results are given in Table 10 and are shown graphically in Figure 8. Photoionisation rates, Γ, were taken from Keenan (1984) and the recombination coefficients, α, from Aldrovandi & Péquignot (1973). Inspection of Figure 8 shows that, while the errors are large, with $< n_e >$ being uncertain by about two orders of magnitude, the different pairs of ions generally give values that are consistent with each other.

Table 10
Mean electron densities determined from successive ionisation stages for the Sco OB1 sightline. Units are cm^{-3}.

Star HD	Log $< n_e >$ (Mg I/Mg II)	Log $< n_e >$ (C I/C II)	Log $< n_e >$ (S I/S II)
151804	$+0.10^{+0.85}_{-1.50}$	$-0.59^{+1.03}_{-0.84}$	$+0.19^{+0.14}_{-0.15}$
152234	$-0.32^{+0.90}_{-1.20}$	$-1.21^{+0.66}_{-0.68}$	$-0.43^{+0.21}_{-0.32}$
152235	...	$< +0.09$	$-0.06^{+0.69}_{-0.99}$
152236	$-0.48^{+1.00}_{-1.11}$	$< +1.40$	$-0.88^{+0.48}_{-0.73}$
152408	$+0.55^{+0.67}_{-1.16}$	$-1.03^{+0.92}_{-1.09}$	$-0.99^{+0.35}_{-0.58}$
152424	$-0.11^{+0.59}_{-0.88}$	$-1.64^{+1.04}_{-0.66}$	$-0.34^{+0.19}_{-0.33}$

It is possible to use these electron densities to estimate the space density of hydrogen nuclei, $n_H = n(\mathrm{H\ I}) + 2n(\mathrm{H_2})$, in the absorbing regions. Since carbon is the only abundant heavy atom with an ionisation potential less than 13.6 eV, it will provide the overwhelming majority of the free electrons in diffuse clouds (*i.e.* $n_e \sim n_C$). If we equate the ratio of the C and H column densities (related to the carbon depletion through Equation 5) with the fractional gas phase C abundance in the region of interest we may write:

$$n_e \sim n_C = \left[\frac{N(\mathrm{C})}{N(\mathrm{H})}\right] \times n_H. \qquad (7)$$

Using the carbon depletion factors given in Table 8, this results in n_e values much smaller than those shown in Figure 8 unless $n_H \gtrsim 100$ cm^{-3}. For example, the *minimum* carbon depletions (*i.e.* maximum gas-phase abundance) found for HDs 152234, 152408 and 152424 correspond to $\log(n_e) \sim -1.4$ for $n_H = 100$ cm^{-3}, with higher densities giving proportionately greater values of n_e.

7.2 Gas pressures determined from hyperfine excitation of C I

The relative populations of the C I ground-state hyperfine levels are sensitive to the local temperature and density within the interstellar gas. The level populations are maintained mostly by balance between collisions (both upwards and downwards) with hydrogen atoms and molecules, and by radiative decay. At low pressures there is a small contribution by optical pumping due to the interstellar radiation field. Jenkins & Shaya (1979) have calculated the relative fractional abundance ratios $n(\mathrm{C\ I^*})/n(\mathrm{C\ I_{total}})$ and $n(\mathrm{C\ I^{**}})/n(\mathrm{C\ I_{total}})$ for a range of temperatures and pressures appropriate for diffuse cloud conditions.

Figure 9 shows Jenkins & Shaya's theoretical curve for an assumed temperature of 80 K. The curve is graduated, on a logarithmic scale, with values of $\mathrm{Log}(P/k)$ in units of cm^{-3} K. The error boxes derived from the observed column densites of C I, C I* and C I** towards the Sco OB1 stars (Table 5) are also shown. All physically real ratios must lie between the heavy dashed line (sloping from lower left towards upper right) and the graduated curve. Different temperatures lead to different curves, but provided the temperatures do not differ by more than a few tens of degrees this difference is small (*cf.* Figure 6 of Jenkins & Shaya 1979).

It is physically possible for observed ratios to lie off the theoretical curve, provided they are to the right of the dashed line. Observed ratios will lie in this region if, as is likely, the sightline intercepts more than one region with different physical conditions. In the special case where two regions contribute, the observed point will lie on a straight line joining the individual points for each region (which do lie on the curve), weighted towards the point representing the region with the greatest column density. Such a line will clearly form a chord to the theoretical curve.

A typical value of $\log(P/k)$ for diffuse interstellar clouds is 3.2, corresponding to $T = 80$ K, $n_H = 20$ cm^{-3} (Spitzer 1978, pp. 163, 227). With the exception of the upper limit obtained for HD 151804 (which results from the non-detection of C I** towards this star), none of the observations are consistent with this low value. It appears that the hyperfine levels of C I in the Sco OB1 sightline are significantly more excited than one would expect for Spitzer's

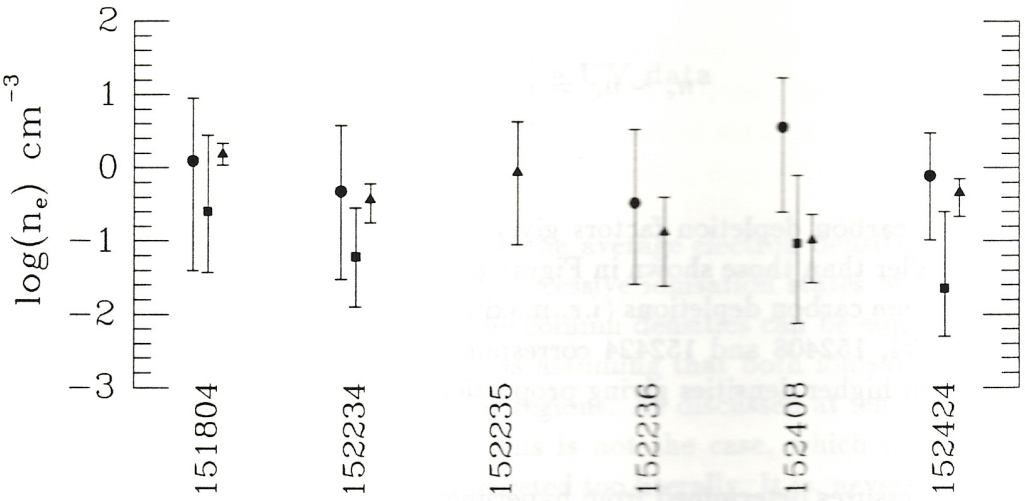

Figure 8. Electron densities determined from the observed column densities of successive ionisation stages; circles, Mg I/Mg II; squares, C I/C II; and triangles, S I/S II.

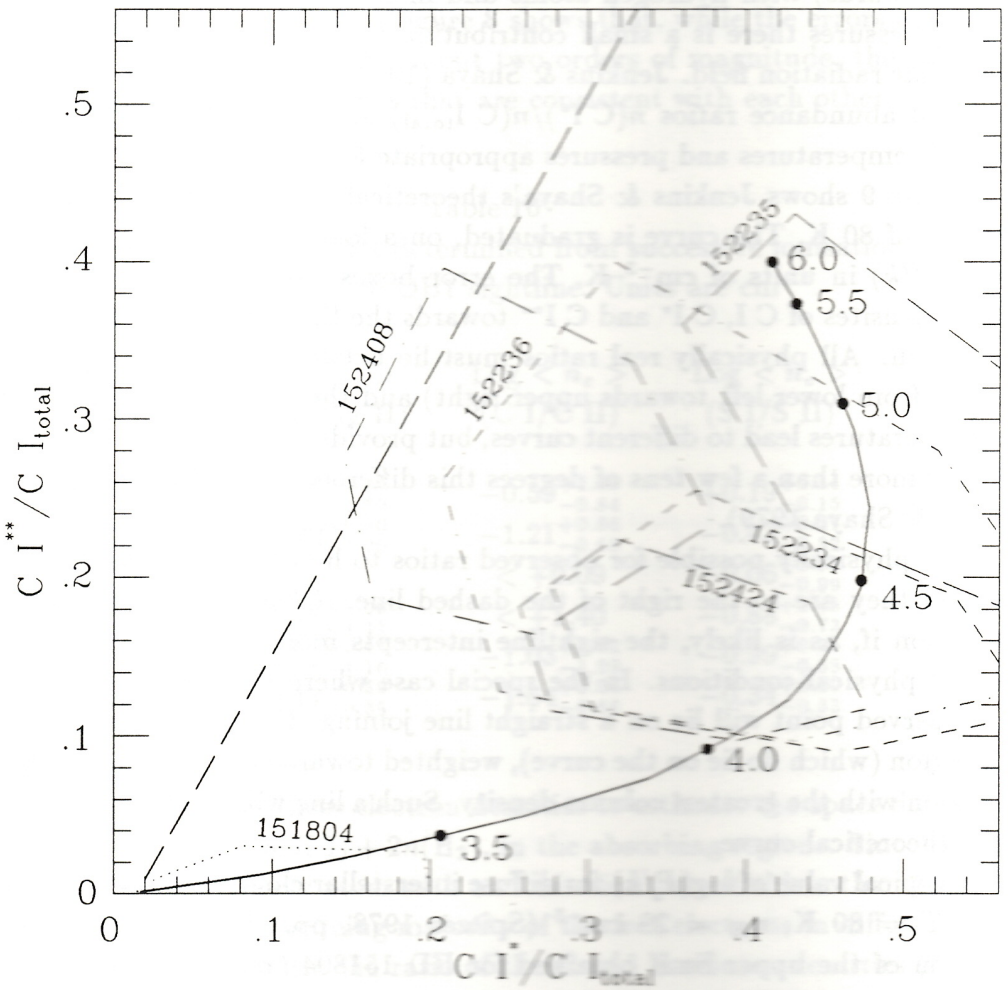

Figure 9. Relative populations of the C I ground state hyperfine levels. The theoretical curve is from Jenkins & Shaya (1979) and assumes a temperature of 80 K. It is graduated in values of $\log(P/k)$. Error boxes correspond to the observed C I column densities for each star. See text for details.

'standard' diffuse clouds. Limits for Log(P/k), estimated by eye from Figure 9 to the nearest 0.05 dex, are given in Table 11 for the case where only one set of physical conditions is responsible for the hyperfine excitation.

Table 11
Pressures, densities and thickness of absorbing material obtained from the excited hyperfine levels of C I. See text for details.

Star HD	Log(P/k) cm^{-3} K	n_H cm^{-3}(80K)	d pc	% line of sight
151804	$\lesssim$3.40	$\lesssim$31	$\gtrsim$17	$\gtrsim$0.89
152234	4.05–4.55	140–440	1.6–5.0	0.08–0.26
152235	$\gtrsim$4.55	$\gtrsim$440	$\lesssim$3.5	$\lesssim$0.18
152236	4.05–5.05	140–1400	1.4–14	0.07–0.74
152408	...	...	...	...
152424	4.05–4.30	140–250	5.1–9.2	0.27–0.48

The values of n_H given in Table 11 are for an assumed temperature of 80 K. Also given, out of interest, are the allowed thicknesses of the material, assuming that all the hydrogen (Table 6) exists at these densities, and the corresponding percentage of each sightline occupied by the material, assuming a distance to the association of 1900 pc. Clearly these will be *upper* limits to the thickness of high density material, since there must be some intercloud hydrogen. It will be seen that for all the sightlines (except possibly that towards HD 151804) gas at the inferred pressure is limited to substantially less than one percent of the total distance to the association.

Although the data for all stars except HD 152408 are consistent with a single set of physical conditions leading to the observed hyperfine excitation, the large areas enclosed by the error boxes (excluding HD 151804) to the left of the curve mean that a mixture of conditions is possible. Given the long sightline to Sco OB1, with all the complex velocity structure observed in the high resolution optical observations (Crawford *et al.* 1989) and the large b values obtained from the curve of growth analysis, this is a more realistic possibility. Indeed, the observed ratios for HD 152408 cannot be explained by a single set of physical conditions, since its error box in Figure 9 does not touch the theoretical curve. However, even if a number of different regions do contribute to the C I hyperfine excitation, the presence of the error boxes in the top right part of the diagram means that most of the C I absorption along each sightline (excluding HD 151804) has occurred at relatively high pressure.

From their sample of 33 stars Jenkins & Shaya (1979) found evidence for pressures greater than 10^4 cm^{-3} K in only a handful of cases. They concluded that gravitational compression in bound clouds was not sufficient to explain

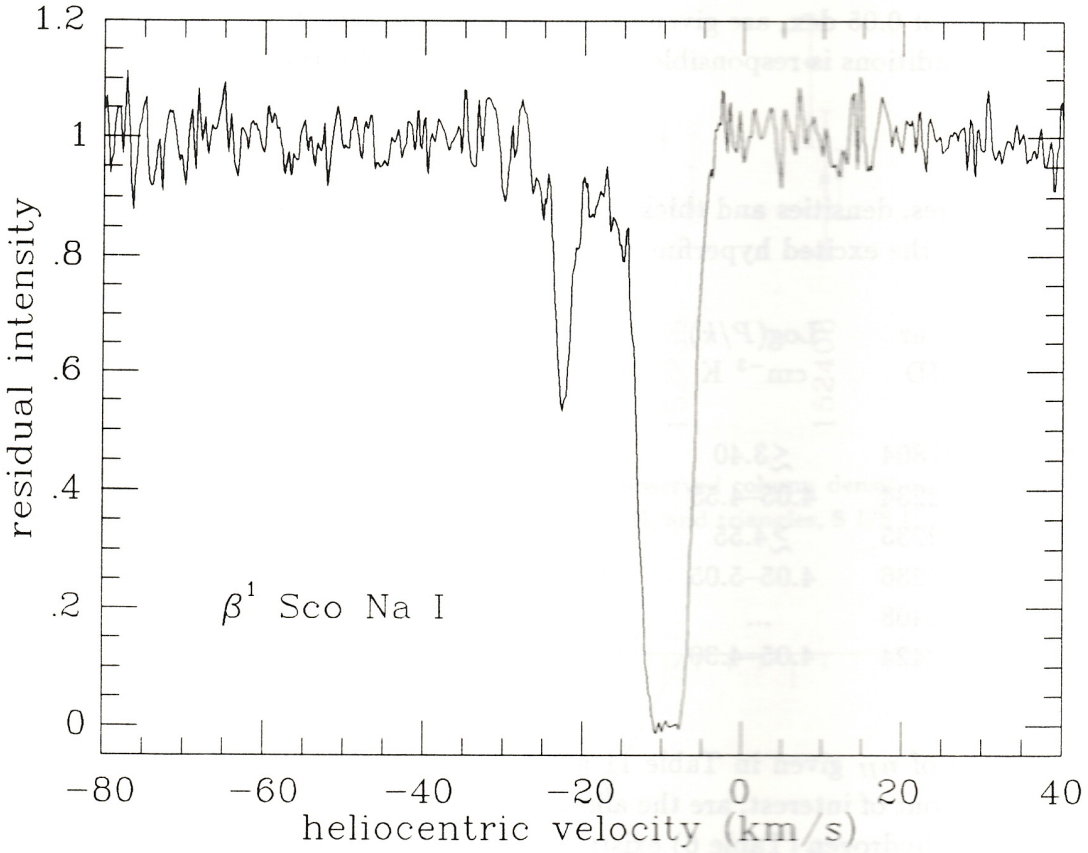

Figure 10. A high resolution spectrum of the interstellar Na D2 line towards β^1 Sco, obtained by Drs. M. J. Barlow and J. C. Blades. Note the absence of highly blue-shifted material ($-50 \lesssim v_{helio} \lesssim -25$ km s^{-1}) of the kind observed towards the Sco OB1 association (Crawford *et al.* 1989).

these few cases, and suggested that energetic phemonena (*e.g.* supernovae and/or stellar mass-loss) might be responsible. They note, in particular, that values of Log(P/k)$\sim$4.5 might occur in dense shells of gas surrounding interstellar bubbles of the type proposed by Castor *et al.* (1975). In the case of Sco OB1, we have strong evidence from the high resolution optical studies (Crawford *et al.* 1989) that an expanding shell of material does surround the association. Although this shell is, at first sight, an obvious location for the high pressure gas, a problem with this interpretation is that C I is expected to have a very similar distribution to Na I along any line of sight. As described by Crawford *et al.* (1989), the *bulk* of the Na I absorption is associated with diffuse interstellar clouds in the foreground, rather than with the shell components. Inspection of Table 3 of Crawford *et al.* (1989) shows that the low velocity components contain between ten and a thousand times as much Na I as the high velocity components. If a similar ratio holds for the distribution of C I, the error boxes shown in Figure 9 should be heavily weighted in favour of the low velocity gas, *i.e.* the foreground diffuse clouds.

Moreover, although Jenkins & Shaya suggested that the high pressures they observed might be due to energetic events surrounding the early-type stars in their sample, one of their clearest examples, β^1 Sco, appears not to be associated with expanding neutral material. Figure 10 shows a high resolution observation of the Na D2 line for β^1 Sco (obtained by Drs. M. J. Barlow and J. C. Blades during the same observing run that produced most of the Na I spectra presented by Crawford *et al.* 1989). It is clear that although β^1 Sco does exhibit a weak Na I component at about -23 km s^{-1}, it is entirely lacking in the strong, highly blue-shifted 'shell' components observed towards Sco OB1. It seems, therefore, that high pressures can exist in the interstellar medium without the presence of high velocity gas, supporting the view mooted above that the high pressures observed towards Sco OB1 originate in one or more of the diffuse clouds intercepted by the line of sight. Note that the existence of relatively high densities (several hundred particles cm^{-3}) in these clouds is consistent with the large electron densities discussed in Section 7.1.

8 Conclusions

An empirical curve of growth analysis of 75 ultraviolet interstellar absorption lines towards six members of the Scorpius OB1 association has resulted in gas-phase abundances for 27 ionic species (Table 5). The effective velocity dispersion parameters obtained from the empirical curves of growth were found to be anti-correlated with stellar reddening (Figure 4) indicating the increasing dominance of narrow, large column density density components towards the more reddened stars. The elemental depletions were found to be generally consistent with those obtained by other authors for diffuse interstellar clouds. Apparently significant density-dependent depletion was found for the atoms Ca, Cr, Mn and Ni (Figure 7). Column density ratios of successive ionisation stages

of Mg, C and S provided estimates of the electron density, although these estimates are uncertain by several orders of magnitude ($-2 \lesssim \log n_e \lesssim +1$; Figure 8) because of saturation of the stronger lines. Note that these electron density estimates are dependent on the assumption that both upper and lower ionisation stages are spatially co-existent, an assumption which cannot be verified with the *IUE* data. Limits on the densities of the interstellar clouds responsible for the absorption were obtained from an analysis of the excitation of the C I hyperfine levels; for all but one star $\log(P/k) \gtrsim 4$ cm^{-3} K, corresponding to $n_H \gtrsim 140$ cm^{-3} at a temperature of 80 K. Owing to the relatively poor velocity resolution of *IUE* (~ 30 km s^{-1}) these values are averages over any unresolved velocity structure. Finally, lines of highly ionised species (C IV, Al III, Si III and Si IV) were also observed. With the exception of C IV, lines from these species were found to be blue-shifted by between about 10 and 30 km s^{-1} relative to the other interstellar lines (Table 4). This is consistent with their formation in an H II region surrounding the OB association. It was suggested that the C IV lines may arise in the hot 'coronal' phase of the interstellar medium.

Acknowledgments

It is a pleasure to thank Dr Derek McNally for his support and encouragement throughout the course of this work. Dr M. J. Barlow read an earlier draft of the manuscript and his comments have greatly clarified the result. I thank the editor of *Communications from the University of London Observatory*, Dr M. M. Dworetsky, for arranging the production of this edition.

References

Aldrovandi, S. M. V. & Péquignot, D., 1973. *Astr. Astrophys.*, **25**, 137.

Aldrovandi, S. M. V. & Péquignot, D., 1974. *Revista Brasileira de Fisica*, **4**, 491.

Barker, P. K., 1984. *Astr. J.*, **89**, 899.

Bertout, C., Leitherer, C., Stahl, O. & Wolf, B., 1985. *Astr. Astrophys.*, **144**, 87.

Black, J. H., Dupree, A. K., Hartmann, L. W. & Raymond, J. C., 1980. *Astrophys. J.*, **239**, 502.

Boggess, A., *et al.*, 1978. *Nature*, **275**, 372.

Bohlin, R. C., Savage, B. D. & Drake, J. F., 1978. *Astrophys. J.*, **224**, 132.

Castor, J., McCray, R. & Weaver, R., 1975. *Astrophys. J.*, **200**, L107.

Cowie, L. L. & Songaila, A., 1986. *Ann. Rev. Astr. Astrophys.*, **24**, 499.

Cowie, L. L., Taylor, W. & York, D. G., 1981. *Astrophys. J.*, **248**, 528.

Crawford, I. A., Barlow, M. J. & Blades, J. C., 1988. *Astrophys. J.*, **336**, 212.

Davenhall, C., 1977. *UCL internal memo.*

Field, G. B., 1974. *Astrophys. J.*, **187**, 453.
Giddings, J., 1983a. *Starlink User Note,* No. 86.
Giddings, J., 1983b. *ESA IUE Newsletter*, **17**, 53.
Gondhalekar, P. M., Phillips, A. P. & Wilson, R. 1980. *Astr. Astrophys.*, **85**, 272.
Grevese, N., 1984. *Phys. Scripta*, **T8**, 49.
Hibbert, A., Dufton, P. L. & Keenan, F. P., 1985. *Mon. Not. R. astr. Soc.*, **213**, 721.
Howarth, I. D. & Murray, J., 1988. *Starlink User Note,* No. 50.
Howarth, I. D. & Phillips, A. P., 1986. *Mon. Not. R. astr. Soc.*, **222**, 809.
Jenkins, E. B. & Shaya, E. J., 1979. *Astrophys. J.*, **231**, 55.
Jenkins, E. B., Savage, B. D. & Spitzer, L., 1986. *Astrophys. J.*, **301**, 355.
Keenan, F. P., 1984. *Mon. Not. R. astr. Soc.*, **206**, 449.
Morton, D. C., 1975. *Astrophys. J.*, **197**, 85.
Morton, D. C., 1978. *Astrophys. J.*, **222**, 863.
Phillips, A. P., Gondhalekar, P. M. & Pettini, M., 1982a. *Mon. Not. R. astr. Soc.*, **200**, 687.
Phillips, A. P., Gondhalekar, P. M. & Pettini, M., 1982b. *Proc. 3rd. European IUE Conf.*, ESA SP-176; p. 415.
Phillips, A. P., Pettini, & Gondhalekar, P. M., 1984. *Mon. Not. R. astr. Soc.*, **206**, 337.
Savage, B. D., 1987. In *Interstellar Processes* (eds. D. J. Hollenbach & H. A. Thronson) Reidel, Dordrecht; p. 123.
Shull, J. M. & Van Steenberg, M. E., 1985. *Astrophys. J.*, **294**, 599.
Spitzer, L., 1985. *Astrophys. J.*, **290**, L21.
Spitzer, L. & Jenkins, E. B., 1975. *Ann. Rev. Astr. Astrophys.*, **13**, 133.
Van Steenberg, M. E. & Shull, J. M., 1988. *Astrophys. J. Suppl.*, **67**, 225.